

# Asymmetries in tropical rainfall and circulation patterns in idealised CO<sub>2</sub> removal experiments

Robin Chadwick · Peili Wu · Peter Good · Timothy Andrews

Received: 11 October 2011 / Accepted: 7 January 2012 / Published online: 29 January 2012  
© Crown Copyright 2012

**Abstract** Atmospheric CO<sub>2</sub> removal is currently receiving serious consideration as a supplement or even alternative to emissions reduction. However the possible consequences of such a strategy for the climate system, and particularly for regional changes to the hydrological cycle, are not well understood. Two idealised general circulation model experiments are described, where CO<sub>2</sub> concentrations are steadily increased, then decreased along the same path. Global mean precipitation continues to increase for several decades after CO<sub>2</sub> begins to decrease. The mean tropical circulation shows associated changes due to the constraint on the global circulation imposed by precipitation and water vapour. The patterns of precipitation and circulation change also exhibit asymmetries with regard to changes in both CO<sub>2</sub> and global mean temperature, but while the lag in global precipitation can be ascribed to different levels of CO<sub>2</sub> at the same temperature state, the regional changes cannot. Instead, ocean memory and heat transfer are important here. In particular the equatorial East Pacific continues to warm relative to the West Pacific during CO<sub>2</sub> ramp-down, producing an anomalously large equatorial Pacific sea surface temperature gradient and associated rainfall anomalies. The mechanism is likely to be a lag in response to atmospheric forcing between mixed-layer water in the east Pacific and the sub-thermocline water below, due to transport through the ocean circulation. The implication of this study is that a CO<sub>2</sub> pathway of increasing then decreasing atmospheric CO<sub>2</sub> concentrations may lead us to climate states during CO<sub>2</sub> decrease that have not been experienced during the increase.

**Keywords** CO<sub>2</sub> removal · Rainfall · Tropical circulation · Geoengineering

## 1 Introduction

The response of the global water cycle to rising temperature and increasing greenhouse gases is likely to provide one of the most significant impacts of climate change on humans, due to societal vulnerability to drought and flooding. Several aspects of the change in precipitation simulated by general circulation models (GCMs), such as a global mean increase in precipitation under warming and the ‘rich get richer’ mechanism whereby wet regions get wetter and dry regions get drier, appear to be robust across models and supported by sound physical principles (Held and Soden 2006; Seager et al. 2010; Chou et al. 2009; Chou and Neelin 2004). However the regional pattern of precipitation change varies widely across GCMs. For example the form that future rainfall changes will take in the tropical Pacific is one area of major disagreement among models (Liu et al. 2005; DiNezio et al. 2009). This is important as rainfall-related diabatic heating from this region (and its variability in the form of the El Niño Southern Oscillation (ENSO)) has a major effect on global weather and climate. Differences in the Sea Surface Temperature (SST) pattern response to global warming may well explain a large proportion of the difference in tropical precipitation patterns across models (Xie et al. 2010), and may even contribute to differences in the global mean precipitation response (Barsugli et al. 2006).

Removal of CO<sub>2</sub> from the atmosphere is currently receiving significant political and media attention as a possible supplement to or even replacement for emissions reduction. Several recent studies have examined the effect

---

R. Chadwick (✉) · P. Wu · P. Good · T. Andrews  
Met Office Hadley Centre, Exeter, UK  
e-mail: robin.chadwick@metoffice.gov.uk

that geoengineering projects might have on global precipitation, including the effects of removing CO<sub>2</sub> from the atmosphere or reducing the amount of incoming solar radiation incident on the Earth's surface (Wu et al. 2010; Cao et al. 2011; Jones et al. 2010; Bala et al. 2008, 2010; Ricke et al. 2010). While reduction of incoming solar radiation could lead to unpredictable, undesirable effects on the climate, particularly on the hydrological cycle (Robock et al. 2008; Bala et al. 2010; Ricke et al. 2010), atmospheric CO<sub>2</sub> removal is widely seen as a safer option, analogous with treating the cause rather than the symptoms of the problem. The assumption here has generally been that the climate response is exactly reversible under CO<sub>2</sub> removal, but this is in fact unlikely to be the case.

Wu et al. (2010) examined an idealised GCM experiment whereby CO<sub>2</sub> was ramped up to 4 times pre-industrial levels, then ramped down to its original value. They found that global mean precipitation increases during the ramp-up phase (as expected), but that it continues to increase for several decades after CO<sub>2</sub> starts to decrease. This hydrological hysteresis can be explained by the dependence of global mean precipitation on the tropospheric radiation budget (via latent heat release). As well as being affected by temperature changes, this budget is also directly influenced by the amount of CO<sub>2</sub> present in the atmosphere, with the direct effect of CO<sub>2</sub> being to suppress precipitation (Andrews et al. 2009). During the ramp-down phase the decrease in temperature lags CO<sub>2</sub> due to the large heat capacity of the ocean. So two states with the same temperature, one during ramp-up and one during ramp-down, will have different CO<sub>2</sub> concentrations and therefore different global mean precipitation (Cao et al. 2011).

Studies to date have focused on global mean precipitation changes under CO<sub>2</sub> ramp-up/ramp-down scenarios, and their constraint by global-mean energy budget arguments. These global changes are likely to be associated with regional precipitation changes with the potential to have large human impacts. The purpose of this paper is to describe and analyse regional patterns of precipitation and circulation change during CO<sub>2</sub> ramp-up/ramp-down experiments, and to look for possible physical mechanisms for these changes. The focus will be on the tropical Pacific as this is where the largest changes in rainfall occur.

The regional distribution of tropical rainfall is intimately connected to the large-scale tropical circulation, and any rainfall changes are likely to be associated with circulation changes. Held and Soden (2006) showed that  $P = Mq$ , where  $P$  is precipitation,  $M$  is mass flux from the boundary layer into the free troposphere, and  $q$  is a typical boundary layer mixing ratio. If constant relative humidity is assumed, then  $q$  is determined by  $T$  (global mean temperature). So two states with equal  $T$  but differing  $P$  (i.e. CO<sub>2</sub> ramp-up

and ramp-down states) must have different values of  $M$ , implying a change in convective mass flux and circulation during CO<sub>2</sub> ramp-up/down that is not symmetric about the points of either maximum CO<sub>2</sub> or maximum  $T$ . This change in the magnitude of circulation could either simply weaken or reinforce the existing circulation pattern, or else lead to changes in the position of ascent and descent regions. If the second case is true then this would have more profound consequences for changes in regional precipitation.

This paper begins by describing the GCM experiments used to examine the climate response to CO<sub>2</sub> ramp-up/ramp-down. Next, the transient pattern of precipitation and surface temperature responses during the experiments are described and analysed. Following this, an ocean dynamical mechanism for the asymmetric changes in Pacific SSTs and rainfall is proposed, and is then related to changes in the tropical circulation. The sensitivity of these results to the maximum CO<sub>2</sub> concentration during ramp-up/ramp-down is then explored. Finally, the linearity of the pattern response to CO<sub>2</sub> ramp-up/ramp-down is investigated using a simple linear climate model.

## 2 Experimental setup

Two CO<sub>2</sub> ramp-up/ramp-down GCM runs, using two different Hadley Centre coupled climate models, were available for this analysis. The first experiment used the HadCM3 model (Gordon et al. 2000) and is described in Wu et al. (2010). The atmospheric component has a horizontal resolution of 2.5° lat, 3.75° lon, with 19 vertical levels. The ocean component has a resolution of 1.25° by 1.25° with 20 vertical levels.

CO<sub>2</sub> was increased at 2% per year from pre-industrial values (280 ppm) until quadrupling (1,120 ppm) after 70 years. CO<sub>2</sub> concentrations were then stabilised for 10 years before decreasing at 2% per year back to pre-industrial levels. There then followed a stabilisation period of 150 years at pre-industrial CO<sub>2</sub> levels.

The second experiment used the higher resolution and more complex HadGEM2-ES (Hadley Centre Global Environmental Model version 2 Earth System model). HadGEM2-ES (Martin et al. 2011; Collins et al. 2011) is a coupled atmosphere–ocean–sea ice model combined with component models for atmospheric aerosols, tropospheric chemistry, and terrestrial and oceanic ecosystems involved in various couplings within the Earth system. The atmospheric component has a horizontal resolution of 1.25° lat, 1.875° lon, with 38 vertical levels. The ocean component has a resolution of 1° by 1° between the poles and 30°S and 30°N, with resolution increasing smoothly to 1/3° at the equator. There are 40 unevenly spaced levels in the vertical.

The experiment is described in Boucher et al. (2011), and involved increasing CO<sub>2</sub> at 1% per year from pre-industrial concentrations until quadrupling after 140 years. CO<sub>2</sub> was then reduced at 1% per year until returning to pre-industrial levels. CO<sub>2</sub> levels were prescribed for this experiment, so CO<sub>2</sub> fluxes between the atmosphere and the ocean, and between the atmosphere and the land surface are diagnostics only.

Three other HadGEM2-ES CO<sub>2</sub> ramp-up/ramp-down experiments were also analysed. These also increased and decreased at 1% per year from pre-industrial concentrations but peaked at varying CO<sub>2</sub> levels ( $3 \times \text{CO}_2$ ,  $2 \times \text{CO}_2$  and  $1.5 \times \text{CO}_2$ ). The HadGEM2-ES and HadCM3  $4 \times \text{CO}_2$  experiments are the main focus of this paper, as they have the largest change in radiative forcing and are therefore likely to show the strongest signal of change. The other ramp-up/ramp-down experiments are used to establish the sensitivity of results to the magnitude of forcing.

We also make use of an abrupt  $4 \times \text{CO}_2$  step-up and control experiment with HadGEM2-ES, but this time the ocean and sea-ice model are replaced with climatological SSTs, di-methyl sulphide (DMS) fluxes and sea-ice distributions. These climatologies are derived from a stable fully-coupled pre-industrial control integration. In this setup the atmosphere is free to respond to the change in atmospheric radiative heating caused by the increased CO<sub>2</sub>, but surface temperatures are held fixed (e.g. Hansen et al. 2005). We refer to this as the ‘Hansen’ experiment.

We use this the Hansen experiment to separate the CO<sub>2</sub> direct radiative effect on precipitation from that associated with large-scale changes in surface temperature (e.g. Bala et al. 2010; Andrews et al. 2010). In transient situations it is important to realise that these two effects emerge on different timescales due to the relatively small heat capacity of the atmosphere compared to the ocean. Note that in HadGEM2-ES CH<sub>4</sub> and O<sub>3</sub> are usually calculated by the tropospheric chemistry model, but in these Hansen experiments the interactive CH<sub>4</sub> and O<sub>3</sub> are uncoupled from the radiation code, which sees prescribed climatological values. This was done in order to enable easier implementation of the Coupled Model Intercomparison Project phase 5 (CMIP5) design.

Control runs with fixed pre-industrial CO<sub>2</sub> levels were used for both HadCM3 and HadGEM2-ES. The HadGEM2-ES control had no noticeable drifts in the variables of interest, so a 50 year mean was taken of the control run and used as a comparison for the experimental values and to calculate anomalies from. The HadCM3 control has a drift in the thermohaline circulation and Atlantic ocean temperatures. Although this does not lead to a noticeable drift in global mean temperature, parallel segments of the control run were used to calculate anomalies for the HadCM3 experiment.

Pennell and Reichler (2011) found that of all the pairs of GCMs originating from the same modelling centre, HadCM3 and HadGEM1 (the predecessor of HadGEM2) were the least similar to one another. This gives some encouragement that any agreement between these two models is an indication of robustness, particularly as the earth-system component of HadGEM2-ES makes it even less similar to HadCM3 than HadGEM1 is.

### 3 Results

#### 3.1 Transient patterns of precipitation and SST change

Figure 1a, b show the behaviour of global mean  $T$  (1.5 m temperature) and  $P$  for HadGEM2-ES and HadCM3 during CO<sub>2</sub> ramp-up/ramp-down. It can be seen that precipitation in both models continues to increase for several decades after both CO<sub>2</sub> and temperature have peaked. The lag is longer in HadCM3, possibly because the change in forcing is more abrupt (2% per year as opposed to 1% per year for HadGEM2-ES), because of the 10 year stabilisation at peak CO<sub>2</sub>, or else because the non-linear effect of CO<sub>2</sub> and temperature on precipitation is stronger in HadCM3 than in HadGEM2-ES (Good et al. 2011a).

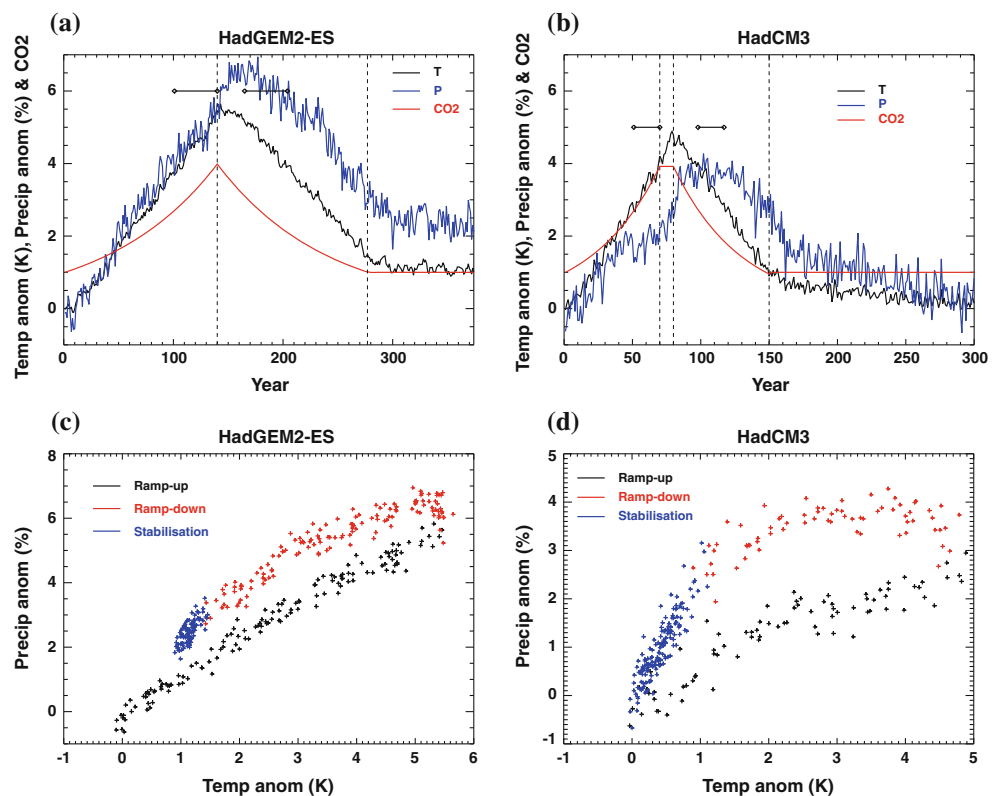
After CO<sub>2</sub> stabilisation  $T$  remains higher than its original state and decreases only slowly. It is presumed that  $T$  would return to its original level if a long enough stabilisation period were applied (at pre-industrial CO<sub>2</sub> forcing) that the deep ocean could release all heat stored during the perturbed forcing period. Change in precipitation plotted against temperature is shown in Fig. 1c, d. This illustrates the possibility of multiple  $P$  states for the same  $T$  due to the direct dependence of  $P$  on CO<sub>2</sub> (Cao et al. 2011).

Global mean  $T$  is often taken as a measure of the severity of a climate anomaly, but in this case it is clear that changes in global mean  $P$  do not scale with  $T$ . As the impacts of precipitation changes depend heavily on the pattern of change, it is of interest how regional precipitation varies with  $T$  and CO<sub>2</sub> during CO<sub>2</sub> ramp-up/ramp-down.

Figures 2a, b and 3a, b show multi-annual mean anomalies of precipitation, for ramp-up and ramp-down periods chosen to be symmetric about the point of maximum CO<sub>2</sub>. As well as the magnitude of global  $P$  being asymmetric about maximum CO<sub>2</sub>, the pattern of precipitation anomaly development also appears to be asymmetric about this point, particularly in the tropical equatorial Pacific where a positive precipitation anomaly continues to develop in the ramp-down period.

For HadGEM2-ES these differences become clearer when changes in the circulation are observed. Figure 2c, d

**Fig. 1** Global mean 1.5 m temperature (K) and precipitation (%) anomalies and CO<sub>2</sub> concentration (factor with respect to pre-industrial levels) for **a** HadGEM2-ES and **b** HadCM3 ramp-up/ramp-down experiments. **c** (HadGEM2-ES) and **d** (HadCM3) show precip anomalies against temperature anomalies for the same experiments. *Dashed vertical lines* show boundaries of CO<sub>2</sub> ramp-up/ramp-down periods. *Horizontal diamond-ended lines* in **a** and **b** signify the position of two time periods with the same climatological global mean  $T$ . Similar figures for HadCM3 and HadGEM2-ES respectively are shown in Wu et al. (2010) and Boucher et al. (2011)



show the development of 500 hPa convective updraught mass flux ( $M_c$ ) anomalies during ramp-up/ramp-down in HadGEM2-ES. As expected from physical arguments (Held and Soden 2006; Knutson and Manabe 1995), warming causes a decrease in  $M_c$  in the majority of tropical convective regions. Any increase in precipitation in these regions (e.g. over the maritime continent) is attributed to increased atmospheric water vapour (the thermodynamic component of precipitation change; c.f. Seager et al. 2010). The exception to the general decrease in  $M_c$  is the equatorial Pacific where an increase in  $M_c$  is observed, leading to a positive dynamical component of precipitation change in this region. This increase in  $M_c$  starts to develop during the ramp-up phase, but is asymmetric about maximum CO<sub>2</sub> and stronger during ramp-down than ramp-up. As will be shown later, these equatorial Pacific changes are asymmetric about the change in global mean  $T$  as well as CO<sub>2</sub>.  $M_c$  was not available as a diagnostic from the HadCM3 experiment so cannot be shown here.

Figures 2e, f and 3c, d show the development of surface temperatures during ramp-up/ramp-down. As in the case of precipitation there is an asymmetry about maximum CO<sub>2</sub>. Perhaps the most striking feature in both models is the hemispheric asymmetry due to a contrast between the speeds of thermal response of land and ocean to CO<sub>2</sub> forcing. This will be discussed in more detail in Sect. 3.2 but does not appear to be the main contributor to the tropical Pacific precipitation anomalies. For HadGEM2-ES

(Fig. 2e, f) one obvious feature is a relative warming of the east and central equatorial Pacific. This persists throughout CO<sub>2</sub> ramp-down and into the stabilisation period (not shown). In HadCM3 (Fig. 3c, d) a similar though less pronounced pattern is present. Only two time-slices are shown here for each model, but the evolution of central and east Pacific SST anomalies has been examined and is consistent throughout CO<sub>2</sub> ramp-up/ramp-down, suggesting that the pattern is unlikely to be due to internal multi-decadal oscillations.

As global mean  $T$  lags CO<sub>2</sub> during ramp-down, the difference between the two periods shown in Figs. 2 and 3 will include a signal due to the difference in  $T$  between them (the ramp-down period is warmer than the ramp-up one). In order to eliminate this  $T$  signal and study these rainfall and SST asymmetries in more detail, two 40 year time periods were chosen for HadGEM2-ES. The first period was the last 40 years of CO<sub>2</sub> ramp-up, while the second was chosen to be the 40 year ramp-down period with (approximately) the same climatological mean  $T$  as the first period (these periods are shown on Fig. 1a). In this way any difference between the two periods should be independent of global mean  $T$ , and the difference in global mean  $P$  should be purely a consequence of different CO<sub>2</sub> levels in the two periods (with lower CO<sub>2</sub> and hence higher global mean  $P$  in the second period). As the thermodynamical component of precipitation change should scale with  $q$  and therefore  $T$ , this procedure should isolate

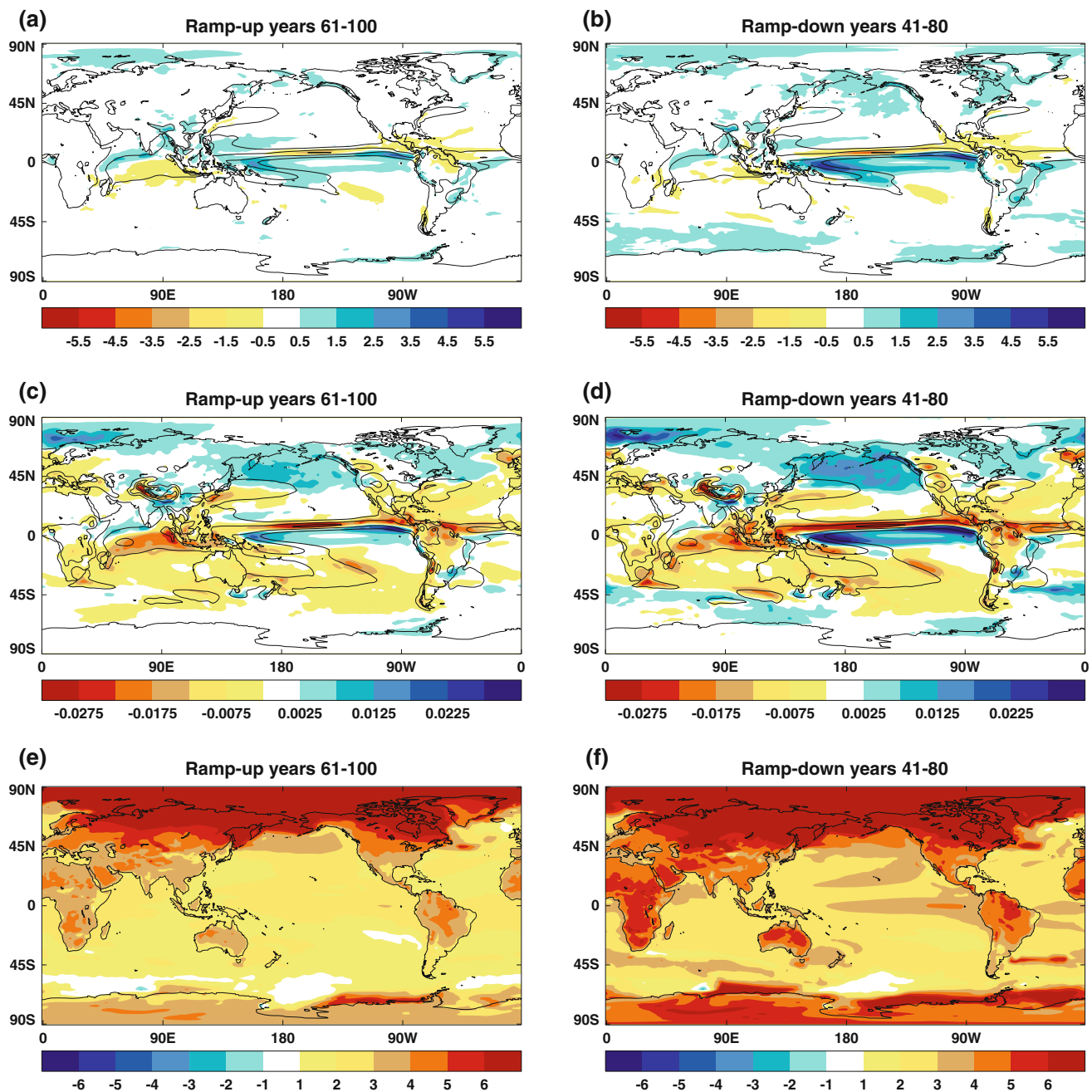


**Fig. 2** HadGEM2-ES anomalies from control for two 40 year means, one during CO<sub>2</sub> ramp-up and one during CO<sub>2</sub> ramp-down and symmetrical about the point of maximum CO<sub>2</sub>. **a, b** Precipitation (mm/day), **c, d** Convective mass flux at 500 hPa (Pa/s) (positive mass

flux is upwards), **e, f** Surface temperature (K). *Line contours* indicate mean control-run values with contour intervals of 5 mm/day for precipitation and 0.05 Pa/s for convective mass flux

dynamical precipitation changes between ramp-up and ramp-down. A similar procedure was followed for HadCM3, but in this case using 20 year periods due to the shorter time and larger forcing gradients in that experiment (see Fig. 1b).

Differences of  $P$  and surface temperature between these periods (ramp-down minus ramp-up) are shown in Figs. 4a, b and 5a, b. A pointwise Student's  $t$  test was performed on

these differences, with a null hypothesis that the two time-series for each point have the same mean. Each point time-series was detrended before performing the test, and points where the null hypothesis was rejected at the 5% confidence level are stippled in Figs. 4 and 5.

The surface temperature response of HadGEM2-ES (Fig. 4a) exhibits several interesting features, including a relative warming in the central and eastern equatorial

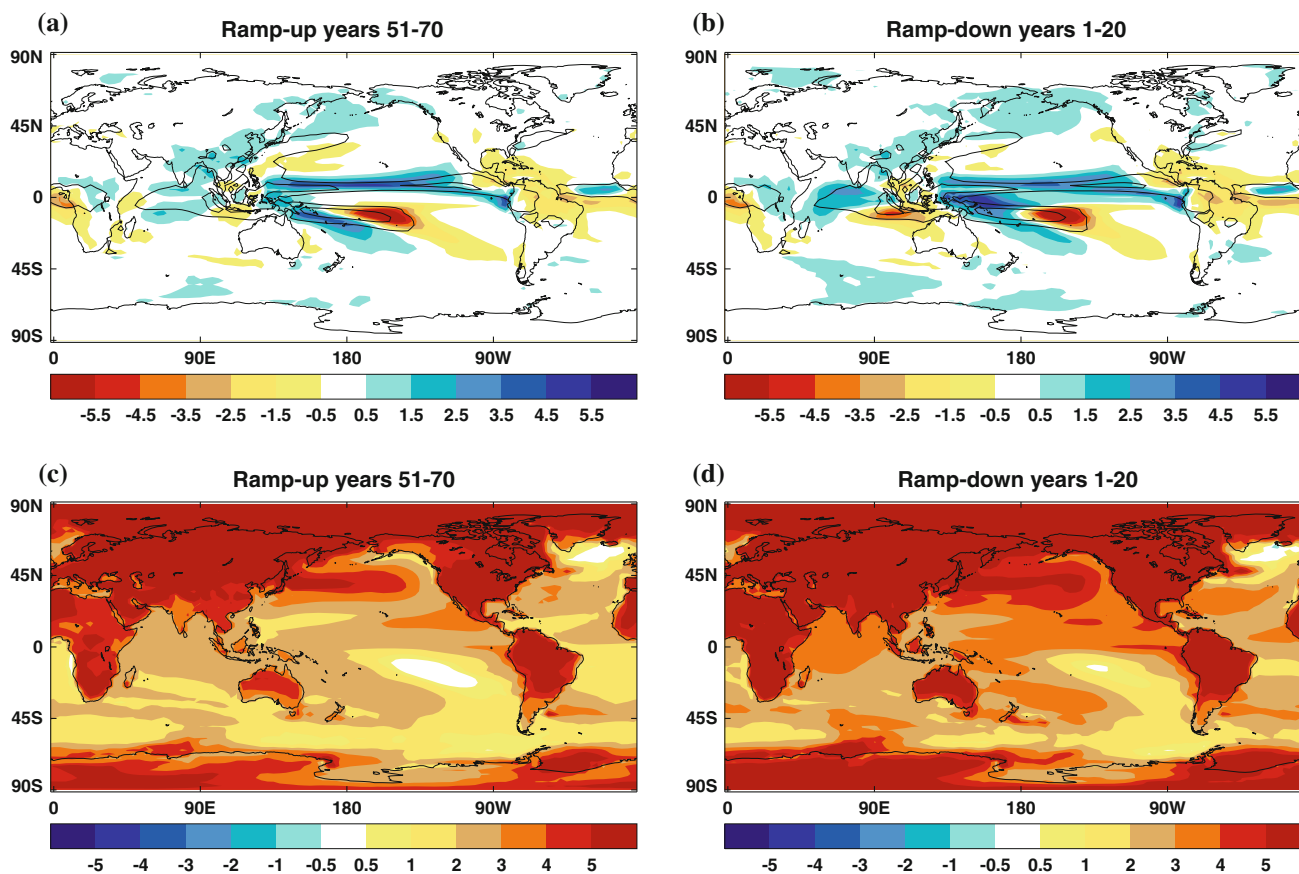


**Fig. 3** HadCM3 anomalies from control for two 20 year means, one during CO<sub>2</sub> ramp-up and one during CO<sub>2</sub> ramp-down and symmetrical about the point of maximum CO<sub>2</sub>. **a, b** Precipitation (mm/day),

**c, d** Surface temperature (K). *Line contours* indicate mean control-run values with contour intervals of 5 mm/day for precipitation

Pacific and a decrease in the equatorial Pacific zonal temperature. HadCM3 shows a similar pattern of surface temperature change to HadGEM2-ES between the two periods of equal mean  $T$  (see Fig. 5), though the equatorial Pacific warm anomaly is much more equatorially confined than in HadGEM2-ES and is located further towards the central Pacific. Although these temperature anomalies are small compared to the amplitude of a typical El Niño anomaly, persistent small amplitude anomalies in the tropical Pacific can have large impacts on global climate (Karnauskas et al. 2009) and are thought to have been responsible for the 1930s North American dust bowl drought (Schubert et al. 2004).

The detailed differences in SST response between HadGEM2-ES and HadCM3 are likely to be a combination of differences in experimental design and differences in the structure, parametrizations and biases of the GCMs, but the broad agreement between the models suggests a degree of robustness to the results.

The rainfall anomalies in Figs. 4b and 5b both show a shift of rainfall into the central and eastern equatorial Pacific similar to that seen during El Niño events, with

associated negative rainfall anomalies in the inter-tropical and south Pacific convergence zones and over the maritime continent. It can be seen from Fig. 4c that for HadGEM2-ES these rainfall anomalies are entirely explained by the change in convective mass flux, identifying them as dynamical precipitation changes.

As the pattern of increased rainfall and  $Mc$  in the central and eastern equatorial Pacific is consistent with circulation changes induced by an East Pacific SST warming (such as in an El Niño event), it seems likely that it is the slowly developing SST patterns that are responsible for the asymmetry of precipitation patterns during ramp-up/ramp-down. This is consistent with the study of Xie et al. (2010) using an ensemble of NCAR (National Center for Atmospheric Research) and GFDL (Geophysical Fluid Dynamics Laboratory) GCMs, who found that tropical precipitation changes are positively correlated with spatial deviations of SST warming from the tropical mean.

However the SST anomalies are not the only possible mechanism for the asymmetry in precipitation patterns. As the lag in global mean  $P$  with respect to  $T$  can be explained by the ‘fast precipitation response’ to CO<sub>2</sub> (Cao et al.

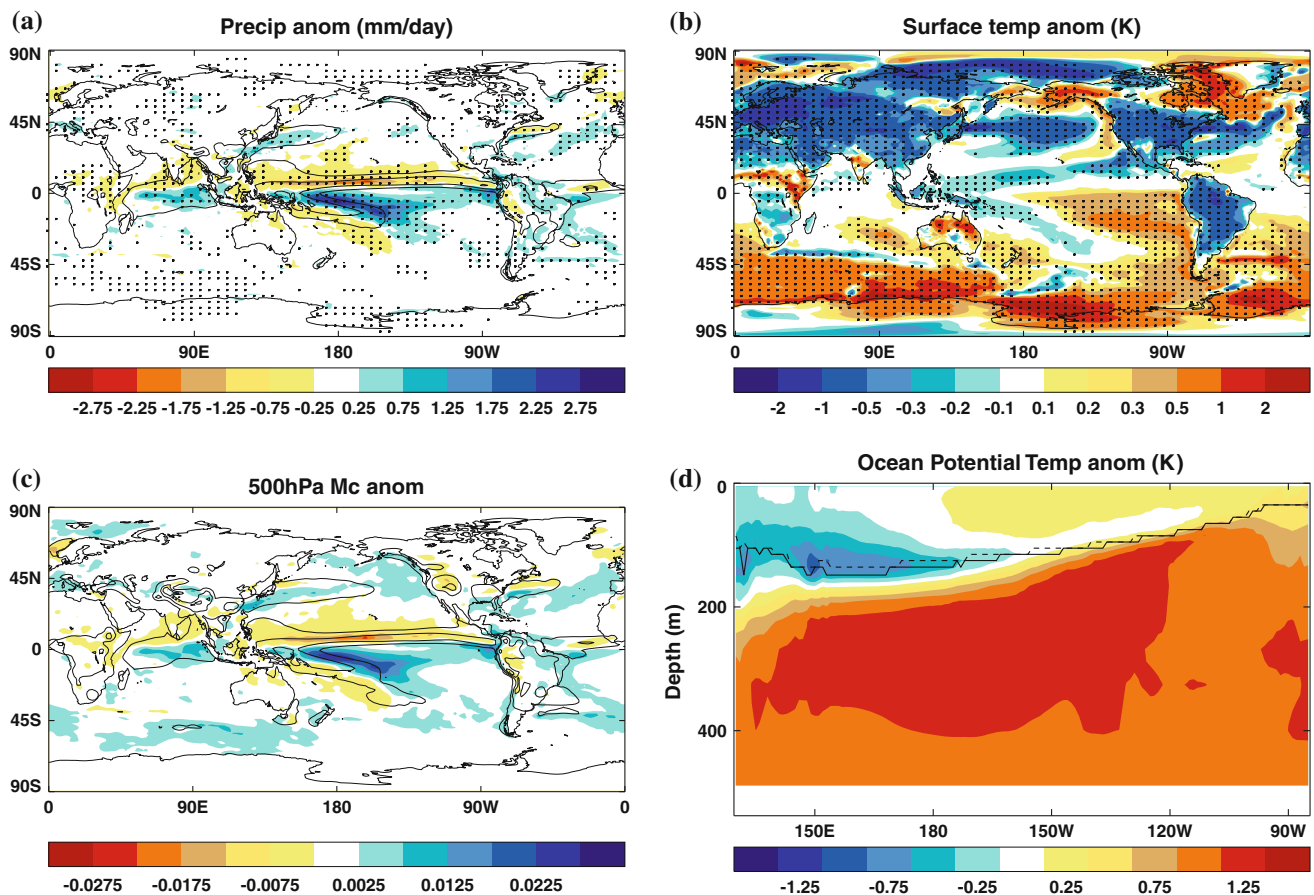


**Fig. 4** Difference (ramp-down minus ramp-up) between two Had-GEM2-ES 40 year time periods, one during ramp-down and one during ramp-up, with the same climatological global mean 1.5 m temperature. **a** Precipitation (mm/day), **b** surface (SST and land surface) temperature (K), **c** updraught convective mass flux at 500 hPa (Pa/s) (positive mass flux is upwards) anomalies. **d** shows the ocean potential temperature anomaly (K) for a cross section of the

Pacific ocean from 5N to 5S. The *solid line* shows the mean thermocline position during the first (ramp-up) period, the *dashed line* shows it during the second (ramp-down) period. In **a** and **b** grid-points where the difference is statistically significant at the 5% level are stippled. *Line contours* indicate mean values during the first 40 year period with contour intervals of 5 mm/day for precipitation and 0.05 Pa/s for convective mass flux

2011), one possibility is that the asymmetries in the pattern of  $P$  between ramp-up and ramp-down might also be due to this effect. This was investigated by looking at the results of an experiment designed to isolate the direct radiative effect of CO<sub>2</sub>.

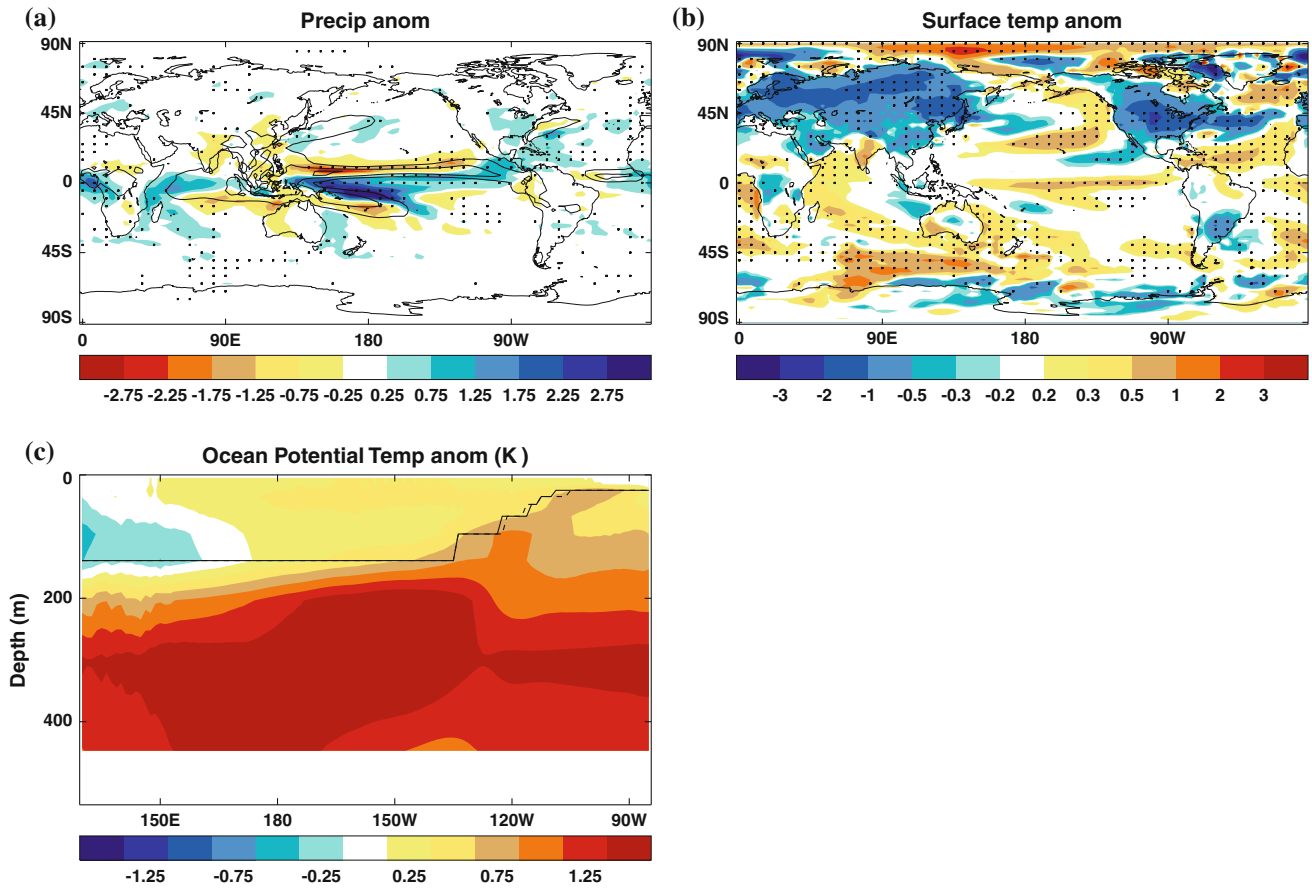
### 3.2 The direct effect of CO<sub>2</sub> on tropical precipitation

Figure 6 shows the results of a ‘Hansen’ experiment, whereby CO<sub>2</sub> is instantaneously quadrupled, but SSTs are held fixed. It should be noted that although SSTs are held constant, the land surface is allowed to heat up. Land surface heating and associated circulation changes are included as part of the fast CO<sub>2</sub> response due to their relatively short timescale of adjustment to forcing.

Figure 6a shows the precipitation response in the Hansen experiment. Over the ocean there is a general reduction in precipitation in convective regions, but no significant

change in the pattern of precipitation (with the exception of a shift of the ITCZ (Inter-tropical convergence zone) on the eastern boundary of the Pacific). The Mc anomaly in Fig. 6b shows that these changes are dynamical, with a suppression of convection across all the main convective centres. This over-ocean stabilisation can be explained by the absorption properties of CO<sub>2</sub> and the overlap of CO<sub>2</sub> absorption lines with water vapour (WV) (Mitchell et al. 1987; Sugi and Yoshimura 2004), combined with a possible shift of rainfall from ocean to land due to enhanced land-sea surface temperature gradients.

The over-ocean precipitation change in the Hansen experiment is one of suppression of existing precipitation regions and the direct effect of CO<sub>2</sub> does not appear to lead to significant spatial redistribution of precipitation. Although non-linear interactions between  $T$  and CO<sub>2</sub> are possible (Good et al. 2011a), and could in theory lead to changes in rainfall patterns in the ramp-up/ramp-down



**Fig. 5** Difference (ramp-down minus ramp-up) between two HadCM3 20 year time periods, one during ramp-down and one during ramp-up, with the same climatological global mean 1.5 m temperature. **a** Precipitation (mm/day), **b** surface (SST and land surface) temperature (K). **c** shows the ocean potential temperature anomaly (K) for a cross section of the Pacific ocean from 5N to 5S. The *solid*

*line* shows the mean thermocline position during the first (ramp-up) period, the *dashed line* shows it during the second (ramp-down) period. In **a** and **b** grid-points where the difference is statistically significant at the 5% level are stippled. *Line contours* indicate mean values during the first 20 year period with contour intervals of 5 mm/day for precipitation

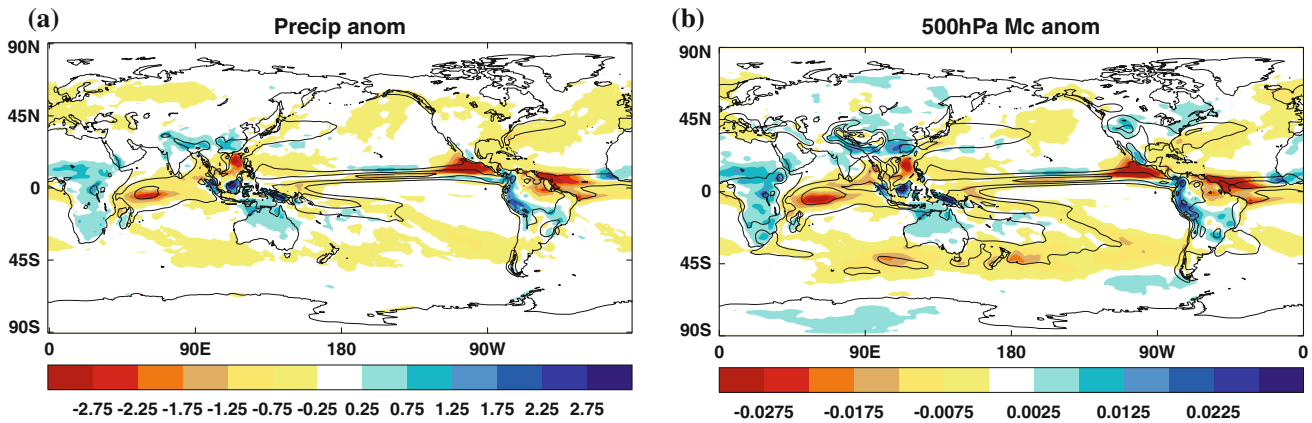


**Fig. 6** Anomalies of **a** Precipitation (mm/day) and **b** updraught convective mass flux at 500 hPa (Pa/s) (positive mass flux is upwards) for the Hansen experiment. The anomalies are constructed by subtracting the mean of the 20 years immediately before CO<sub>2</sub> step-up

from the 20 year mean beginning 10 years after the CO<sub>2</sub> step-up. *Line contours* indicate mean control-run values with contour intervals of 5 mm/day for precipitation and 0.05 Pa/s for convective mass flux



experiment where SSTs are not fixed, they do not seem to play a large role in HadGEM2-ES. It therefore seems likely that although the direct effect of CO<sub>2</sub> on precipitation can explain the global mean lag in  $P$ , the lag and continuing development of oceanic precipitation patterns during ramp-up/ramp-down is not due to the direct radiative effect of CO<sub>2</sub>. The linearity of the changes in  $P$  with regard to  $T$  and CO<sub>2</sub> will be investigated later in this study.

It appears regional redistribution of rainfall during CO<sub>2</sub> ramp-up/ramp-down is caused by circulation changes associated with changing SST gradients, not by direct CO<sub>2</sub>-related rainfall enhancement. This can be seen from the change in  $Mc$  between the two periods in HadGEM2-ES (Fig. 4c). If CO<sub>2</sub> effects were dominant then the pattern of  $Mc$  change should be the opposite of that seen in the Hansen experiment (Fig. 6c), with  $Mc$  increased over convective regions in the second period but no circulation shift. In fact a clear shift in circulation is seen, with increased  $Mc$  in the central and eastern equatorial Pacific and a reduction in  $Mc$  in the ITCZ and SPCZ regions. The positive equatorial Pacific precipitation anomaly extends further west in HadCM3 than in HadGEM2-ES, consistent with the relative SST anomalies in the two models.

As well as changes in the equatorial Pacific, Figs. 4 and 5 show interesting asymmetries in surface temperature and rainfall over land, particularly in the monsoon regions. Some of these can be explained by the direct radiative effect of CO<sub>2</sub> and these will be investigated in a separate paper. One significant feature to note is the hemispheric asymmetry of warming/cooling rates during CO<sub>2</sub> ramp-up/ramp-down, apparently due to the differential speed of land/ocean temperature responses to radiative forcing and the large capacity of the southern ocean to absorb heat. This hemispheric asymmetry could in theory contribute towards the observed southwards shift in the Pacific ITCZ between ramp-up and ramp-down. Although a corresponding southward shift of the Atlantic ITCZ is seen in HadGEM2-ES (Fig. 4), this is not apparent for HadCM3(5).

The Hansen experiment does not show a northward shift of the Pacific ITCZ despite a hemispheric temperature asymmetry caused by allowing the land-surface to warm but not the ocean. This suggests that local Pacific SST gradients are more important than global-scale hemispheric asymmetries in determining the position of the Pacific rainfall bands. This appears to be true in the present-day climate, where the Pacific ITCZ remains north of the equator during boreal winter, and Bain et al. (2011) found that the position of the observed Pacific ITCZ is largely controlled by tropical Pacific SST patterns. Whether or not the hemispheric temperature asymmetry contributes towards the southward shift in Pacific rainfall patterns, it would not explain the eastward shift in precipitation. In contrast, the observed anomalous equatorial Pacific zonal

SST gradient is consistent with the complete pattern of Pacific rainfall anomalies, as similar anomalies are seen during El Niño events.

Figure 7a, b show transient changes in equatorial Pacific zonal SST gradient during CO<sub>2</sub> ramp-up/ramp-down for HadGEM2-ES and HadCM3, with both models showing a decreasing trend in this gradient during ramp-up that continues for several decades into the ramp-down period before starting to recover. In both cases the Pacific SST gradient lags further behind CO<sub>2</sub> change than does global mean  $T$ . The next question to be considered is why this equatorial Pacific SST asymmetry arises between CO<sub>2</sub> ramp-up and ramp-down.

### 3.3 Equatorial Pacific ocean response

The equatorial Pacific is a highly coupled atmosphere–ocean system, and contains a multitude of feedbacks that act to shape SSTs in the region (Collins et al. 2010; Lloyd et al. 2009). This makes the attribution of cause and effect during climate change experiments of SST and circulation anomalies in the equatorial Pacific non-trivial. DiNezio et al. (2009) examined the response of the equatorial Pacific to greenhouse-gas forcing in the CMIP3 ensemble of GCM experiments, and found that the dominant factor in the east Pacific SST response to warming is the balance that emerges between ocean vertical and horizontal heat transport in any particular model. A weaker Walker circulation during warming leads to weaker zonal ocean currents, and a positive dynamical heating of the east Pacific due to reduced lateral heat flux divergence, and this is partly, fully or more than balanced (depending on the model) by an increase in cooling from below caused by increased vertical temperature stratification.

The magnitude of the cooling influence on eastern Pacific SSTs produced by upwelling is determined by two mechanisms. The first is the strength of upwelling, driven by surface winds and measured in this study through the strength of the Walker circulation. The second is the degree of ocean stratification across the thermocline, with larger stratification meaning that the mixed-layer is cooled more for the same upwelling strength. The depth of the thermocline is also an important factor in the efficiency of upwelling, but this is strongly related to the strength of upwelling and surface wind stress. The various factors influencing the efficiency of upwelling-related cooling in the East Pacific are illustrated in a schematic in Fig. 8. In this section, equatorial Pacific thermocline changes during CO<sub>2</sub> ramp-up/ramp-down will be examined, and in the next section this will be linked to changes in the Walker circulation.

One major difference between the equatorial Pacific response to ENSO and to climate change is that in an

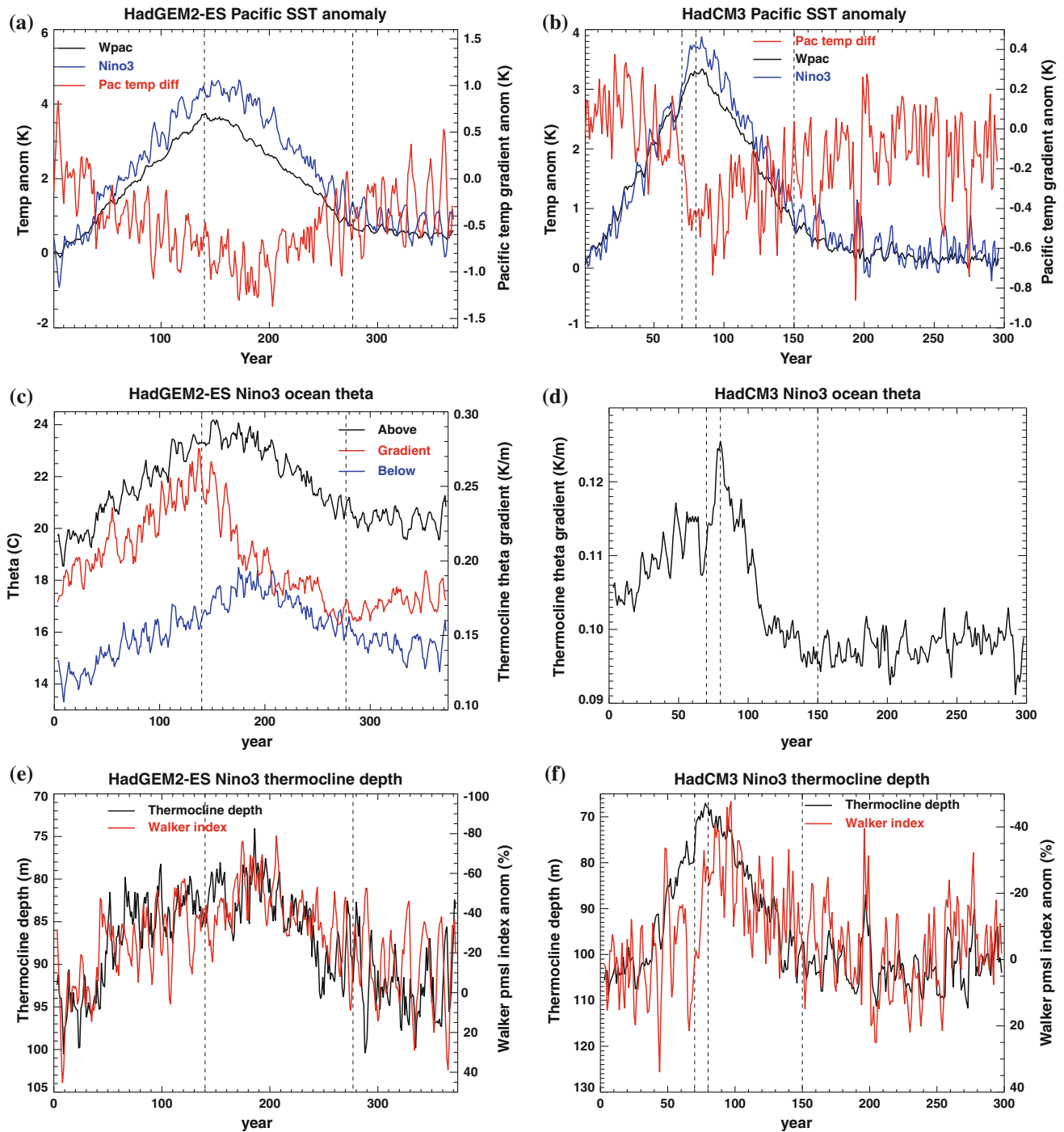


**Fig. 7** Transient changes in mean equatorial West Pacific (5°S–5°N, 80°E–160°W) SST (K), mean equatorial East Pacific SST (K) (Niño3 region, 5°S–5°N, 150°W–90°W) and equatorial Pacific SST gradient (K) (SST difference between the West and East Pacific regions) during CO<sub>2</sub> ramp-up/ramp-down for **a** HadGEM2-ES and **b** HadCM3. **c** shows changes in mean Niño3 thermocline vertical temperature gradient (K/m) for HadGEM2-ES, as well as the mean temperature of the two model levels above the thermocline and the two model levels

below it. **d** shows changes in mean Niño3 thermocline vertical temperature gradient (K/m) for HadCM3. **e** and **f** show changes in mean Niño3 thermocline depth during ramp-up/ramp-down for HadGEM2-ES and HadCM3 respectively, together with the change in Walker circulation index. Note that the Walker circulation index is inverted on the y axis, with positive downwards. All values are filtered using a 5 year moving time window. Dashed vertical lines show boundaries of CO<sub>2</sub> ramp-up/ramp-down periods

ENSO event the Walker circulation is tightly coupled to SST changes, while under climate change the Walker circulation is also controlled by large-scale constraints on the

tropical circulation (Held and Soden 2006). Whereas in an ENSO event SST and Walker circulation changes act to reinforce each other via the Bjerknes feedback, under

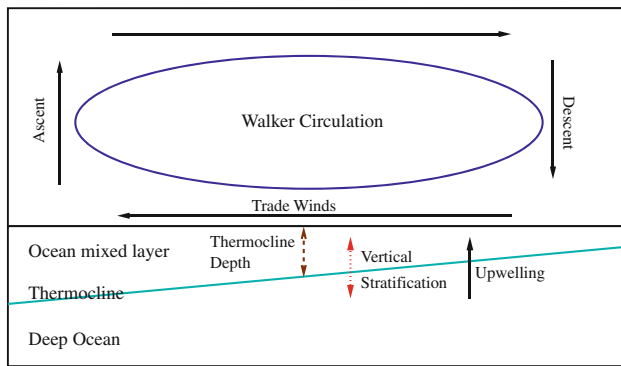


**Fig. 8** Schematic of processes controlling the efficiency of upwelling-related surface cooling in the east Pacific on climate timescales. Equatorial cross-section across the Pacific is shown

climate change it is possible for the Walker circulation and SST gradient changes to be more independent of one another. Karnauskas et al. (2009) discussed the relative roles of competing mean tropical mass flux and local ocean stratification effects on the equatorial Pacific zonal pressure and SST gradients in observations, and found evidence that both effects may already be playing a role in the region. The question here is which mechanism is driving the asymmetry in equatorial Pacific SSTs between CO<sub>2</sub> ramp-up and ramp-down.

The ‘Ocean Thermostat’ mechanism of Clement et al. (1996) predicts a relatively small warming in the east Pacific under greenhouse-gas forcing due to radiative warming of the mixed layer producing enhanced thermal ocean stratification and hence enhanced cooling by upwelling. This effect is complicated in GCMs by the adjustment of the sub-mixed layer water to higher temperatures (Seager and Murtugudde 1997) as heat is transferred into the ocean, but DiNezio et al. (2009) still found that changes in ocean stratification were an important part of the east Pacific mixed-layer heat budget in GCMs.

Figure 7c and d show changes in Niño3 mean thermocline temperature gradient during CO<sub>2</sub> ramp-up/ramp-down. The thermocline gradient is taken as the maximum theta gradient in the top 200 m of the ocean, and so is not dependent upon the absolute depth of the thermocline as it shoals with warming, but remains a good measure of thermal stratification between the mixed-layer and the sub-thermocline waters.

During ramp-up the thermocline gradient increases, and there are two possible explanations for this. The first is the lag between equatorial mixed-layer heating from changes in CO<sub>2</sub> radiative forcing, and CO<sub>2</sub>-related heating of the sub-thermocline ocean. Much of the water which upwells in the east Pacific is originally subducted in the subtropics and eventually feeds into the equatorial undercurrent, with a circulation timescale of decades to centuries (McCreary

and Lu 1994; Matei et al. 2008; McPhaden and Zhang 2002). Therefore water that is present below the east Pacific thermocline during the ramp-up phase will have come into equilibrium with the subtropical atmosphere several decades earlier when CO<sub>2</sub> levels were lower, and will be relatively cool compared to the equatorial mixed-layer.

This would explain a transient increase in stratification as is seen during ramp-up, but DiNezio et al. (2009) also found that the CMIP3 multi-model temperature difference between the surface and 75 m depth remains anomalously high even after over a century of stabilisation. A possible cause of this is that the multi-model mean signal of SST warming is that of enhanced equatorial warming (Liu et al. 2005), with the equator warming more than the subtropics. Therefore the sub-thermocline waters which subduct in the sub-tropics would continue to be relatively cooler than the equatorial mixed-layer waters even at equilibrium. This provides a second possible explanation for the increase in stratification gradient during CO<sub>2</sub> ramp-up. The use of a fixed-depth stratification comparison in the DiNezio et al. (2009) study was necessary in order to compare different models in the CMIP3 ensemble, but means that the result of increased stratification in the raised-CO<sub>2</sub> stable state may be influenced by changes in the depth of the thermocline, as opposed to true changes in the cross-thermocline temperature gradient.

The thermocline theta gradient starts to decrease immediately upon CO<sub>2</sub> ramp-down, and decreases more quickly than it increased (in both HadGEM2-ES and HadCM3). Again this can be explained by the lag between mode water subducting in the sub-tropics and upwelling at the equator. In the ramp-down case, mixed layer water will start to cool from the surface while the temperature of the sub-thermocline water is still increasing, causing a rapid decrease in the sharpness of the thermocline as seen. Figure 7c shows the mean temperature of the two model levels above and mean of the two levels below the thermocline for HadGEM2-ES, and it can clearly be seen that the sub-thermocline waters continue to warm for several decades into the ramp-down. Unlike in HadGEM2-ES, HadCM3 upper ocean model levels are not evenly spaced and changes in thermocline depth during ramp-up/ramp-down mean that the thermocline gradient cannot be interpreted simply as the temperature difference between levels above and below the thermocline. As a result, these temperatures are not shown in Fig. 7d.

The differences in Pacific ocean vertical cross-section theta (potential temperature) between two time periods with equal global-mean  $T$  (one during ramp-up and one during ramp-down) are shown in Figs. 4d and 5c for HadGEM2-ES and HadCM3. These clearly show a relative warming of the deep ocean between these periods, with a

smaller relative warming in the East Pacific mixed layer and relative cooling of the West Pacific mixed layer. The mean depth of the thermocline during the two periods is also shown. For HadGEM2-ES there is a slight shoaling of the thermocline in the second period relative to the first, whereas in HadCM3 no obvious change is seen.

The depth of the thermocline is an important modulator of the efficiency of equatorial upwelling in cooling the surface. Thermocline level is taken here as the model level of maximum vertical theta gradient. Thermocline depth during ramp-up/ramp-down is shown in Fig. 7e and f and follows the trend in Walker circulation strength for both GCMs (the agreement is closer for HadGEM2-ES than for HadCM3). Variations in surface wind stress can cause the thermocline depth to vary (Seager and Murtugudde 1997; Clement et al. 1996), and it is assumed here that on climate timescales changes in thermocline depth are a result of changes in the Walker circulation, not the cause.

### 3.4 Tropical circulation changes

The equatorial Pacific zonal SST gradient is strongly coupled to the strength of the Pacific Walker circulation. As well as this local Pacific coupling, under climate change the tropical circulation weakens as temperature increases (Held and Soden 2006), and this is likely to impact the Walker circulation. In order to try and separate these different drivers of changes in the Pacific Walker circulation, tropical mean convective updraught mass flux ( $M_c$ ) was taken as a measure of the strength of the large-scale tropical circulation. The strength of this large-scale circulation should not be heavily influenced by local Pacific SST changes and can be considered as a measure of the

circulation change due to large-scale precipitation/water vapour constraints. The strength of the zonal mean Hadley cells during CO<sub>2</sub> ramp-up/ramp-down was also examined, in order to compare with that of the Pacific Walker cell.

Figure 9a shows the change in tropical mean (−30°S to 30°N)  $M_c$  integrated between 925 hPa and 100 hPa during ramp-up/ramp-down for HadGEM2-ES ( $M_c$  was not available as a diagnostic from the HadCM3 experiment). A depth integrated value was used as significant changes to the depth of the circulation occurred during ramp-up/ramp-down, so changes in  $M_c$  on a single level reflect changes in circulation depth as well as strength.  $M_c$  decreases during ramp-up, then increases as soon as CO<sub>2</sub> starts to decrease.

Unlike  $T$ ,  $M_c$  does not exhibit a lag with respect to CO<sub>2</sub>, as it is dependent not only on  $T$  but also directly on CO<sub>2</sub> through precipitation and stability changes. This is consistent with the Held and Soden (2006)  $P = Mq$  argument, and this is illustrated by the construction of a proxy for  $M_c$ , denoted  $M_c^*$ .  $M_c^*$  is calculated for each year by dividing  $q$  by  $P$  at each gridpoint, and then taking the tropical mean.  $M_c^*$  is shown in Fig. 9a, and behaves very similarly to  $M_c$ , including its interannual variability. The main difference is that the anomaly in  $M_c$  from control is around 80% of that in  $M_c^*$  throughout the experiment (see Fig. 9b).

This discrepancy could be due to one of several reasons. The assumption in the construction of  $M_c^*$  is that the majority of precipitation in the tropics comes from local mass flux and this assumption of locality may not be entirely valid. Also  $M_c$  is the depth integrated convective mass flux, whereas  $P = Mq$  refers specifically to the total mass flux from the boundary layer to the free troposphere. Another possibility is that sub-annual variability in  $q$  and  $P$  is important. Finally,  $P = Mq$  ignores the return of water

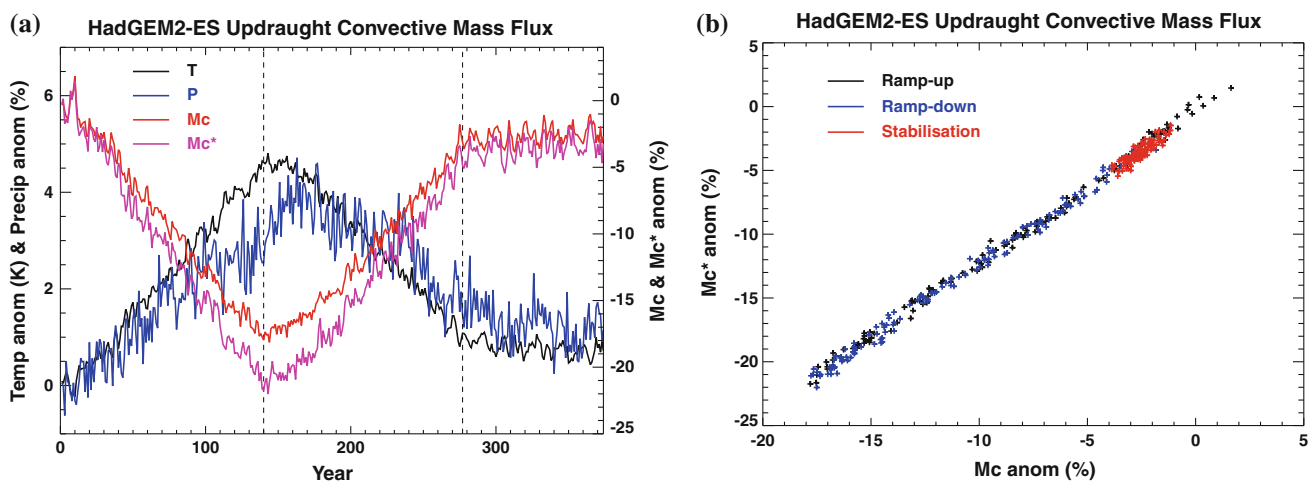


**Fig. 9** **a** Transient change in tropical mean (30°S–30°N) updraught convective mass flux (%) (positive mass flux is upwards) anomaly during CO<sub>2</sub> ramp-up/ramp-down for HadGEM2-ES.  $M_c$  indicates model output mass flux while  $M_c^*$  is proxy mass flux derived from

model  $q$  and  $P$ . Global mean 1.5 m temperature (K) and precipitation (%) anomalies are also shown. **b** shows the relationship between  $M_c$  and  $M_c^*$  during ramp-up, ramp-down and stabilisation. Dashed vertical lines show boundaries of CO<sub>2</sub> ramp-up/ramp-down periods

vapour to the boundary layer in the descending branches of the tropical circulation, and this may not be negligible.

Despite this,  $Mc$  in the model follows the theory of Held and Soden (2006) extremely closely. The consequence of the changes in  $Mc$  is that the strength of the tropical atmospheric circulation should start to recover in strength as CO<sub>2</sub> levels drop, and would not be expected to show a lag as  $T$  and  $P$  do. This does not imply that all aspects of the tropical circulation should behave equally, as a redistribution of the spatial pattern of convection is possible while still satisfying the constraint of tropical mean changes in  $Mc$ .

Figure 10a, b show changes in the strength of the northern Hadley cell in DJF, as measured by the maximum value of the zonally-averaged Stokes' streamfunction (see Trenberth et al. 2000 for a full description of this streamfunction). The changes mirror tropical mean trends in  $Mc$ , with northern Hadley cell strength decreasing during ramp-up (agreeing

with previous studies Gastineau et al. 2009; Held and Soden 2006; Vecchi and Soden 2007), but starting to recover immediately as the ramp-down phase begins.

Interestingly the strength of the southern Hadley cell in JJA shows no noticeable signal throughout ramp-up/ramp-down in either model (not shown), possibly because changes in SST patterns act to maintain the meridional circulation and compensate for global mean  $Mc$  changes in this region and season. Gastineau et al. (2008) examined changes to the Hadley circulation under global warming in the IPSL-CM4 GCM, and found that the Hadley circulation weakened much more in JJA than in DJF. They suggested that changes to the thermohaline circulation in IPSL-CM4 could realign SSTs and produce hemispheric asymmetries in the Hadley cell response to warming in that model. The strength of the JJA Hadley cell is also connected to the strength and position of the Indian monsoon and this is one area where GCMs show limited skill. Therefore

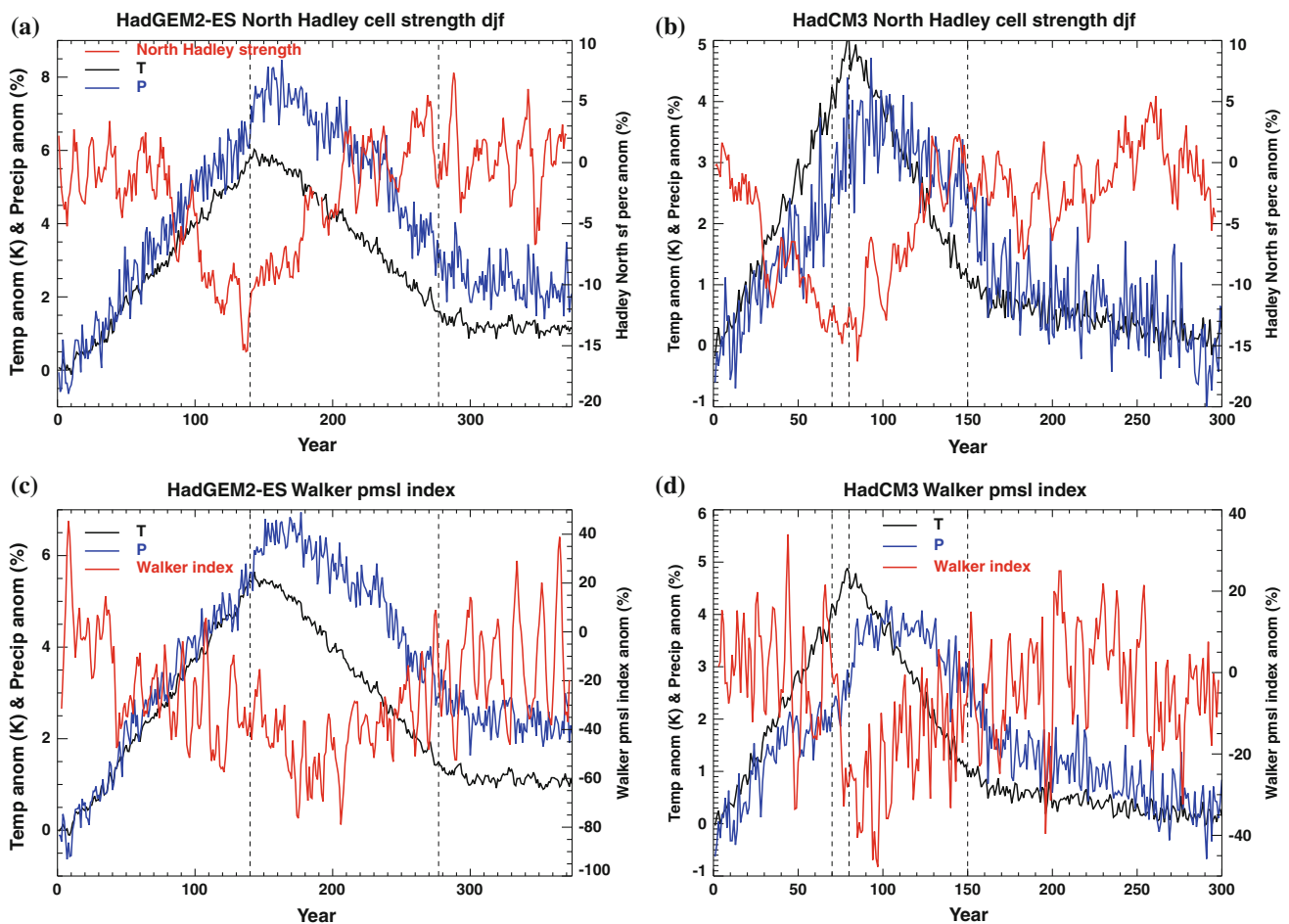


**Fig. 10** Transient circulation strength changes (%) during CO<sub>2</sub> ramp-up/ramp-down. DJF northern Hadley cell strength is shown for **a** HadGEM2-ES and **b** HadCM3. Annual mean Pacific Walker circulation strength is shown for **c** HadGEM2-ES and **d** HadCM3. Global mean 1.5 m temperature (K) and precipitation (%) anomalies

are also shown for all plots (for same seasons as circulation strength). Hadley and Walker circulation strength values are filtered using a 5 year moving window. Dashed vertical lines show boundaries of CO<sub>2</sub> ramp-up/ramp-down periods

model-dependent changes in ocean circulation could produce the different results seen between the Hadley centre models and IPSL-CM4.

Pacific Walker circulation changes are shown in Fig. 10c, d. Following Vecchi and Soden (2007), Walker circulation strength is taken to be the difference in pmsl (pressure at mean sea level) between the eastern Pacific (5°S–5°N, 160°–80°W) and the Indo-west Pacific (5°S–5°N, 80°–160°E). Variations in equatorial Pacific zonal wind stress are highly correlated with this pressure difference index in both models and observations (Vecchi et al. 2006), so it can be considered a proxy for zonal wind stress and the strength of equatorial oceanic upwelling.

Walker circulation strength decreases with warming as expected from previous studies (Vecchi et al. 2006; Vecchi and Soden 2007; Held and Soden 2006; Knutson and Manabe 1995; Gastineau et al. 2009; Zhang and Song 2006), but unlike tropical mean  $\bar{M}_c$  and the Hadley circulation there is a lag between the start of the ramp-down and the Walker circulation beginning to recover. This lag is more pronounced in HadGEM2-ES but is also present in HadCM3. It appears likely that this lag is not caused by tropics-wide changes in  $P$  and  $q$ , but is instead related to local conditions in the equatorial Pacific during ramp-up/ramp-down; specifically temporal asymmetries in SST patterns and the development of an east Pacific warm anomaly. This argument is given weight by the similarity of the length of the lags in Pacific SST gradient and Pacific Walker circulation during the start of CO<sub>2</sub> ramp-down (compare Figs. 7a, b and 10 c, d).

### 3.5 Relative importance of ocean stratification and mean tropical circulation changes

During the ramp-up phase the effect of increasing ocean stratification would suggest a reduced warming of the east Pacific compared to the west Pacific, but in fact the opposite occurs and the East Pacific warms more than the West Pacific (see Fig. 7 a and b). This suggests that the decrease in the strength of the Walker circulation (of up to 40%), and associated weakening of upwelling and zonal ocean currents, dominates over the increased vertical stratification. As the ocean-thermostat effect alone would lead to a La–Niña-like SST pattern and a strengthening of the equatorial pressure gradient, this decrease in the Walker circulation is likely to be driven by constraints on tropical convective mass flux, and the weakening of the mean tropical circulation. Therefore we can ascribe the relative East Pacific warming during ramp-up in HadGEM2-ES and HadCM3 to wider tropical circulation changes related to the argument of Held and Soden (2006).

At the start of ramp-down ocean stratification quickly reduces, while the Walker circulation continues to weaken

for several decades. While both effects would serve to produce an increase in the equatorial Pacific temperature gradient due to a reduction in upwelling-associated cooling, in this case it seems likely that the ocean changes are the driving mechanism which then feeds back into the Walker circulation. During ramp-down, the mean tropical trend is for the atmospheric circulation to strengthen (see Fig. 9), so the tendency of the Pacific Walker circulation to oppose this trend appears likely to be driven by local memory in the system. Due to the small heat capacity of the atmosphere and mixed-layer relaxation time of a few years, the only component in the tropical Pacific with a memory of decades and above is the deep ocean, so it is the continued warming of the sub-thermocline ocean during CO<sub>2</sub> ramp-down that is driving the continuing development of a central and East Pacific SST anomaly and the associated rainfall and circulation changes.

The dominance of different mechanisms during CO<sub>2</sub> ramp-up and the beginning of ramp-down can be explained by the magnitude and speed of stratification change in each case. During ramp-up the tendency is for both the mixed-layer and sub-thermocline ocean to warm, but the mixed-layer warms faster so there is a gradual increase in thermocline gradient (Fig. 7c). However during ramp-down the tendency of the mixed-layer, if disconnected from the deep ocean, would be to cool, while the sub-thermocline waters are still warming due to the lag caused by the ocean circulation. The opposing temperature tendencies lead to a rapid decline in thermocline theta gradient which locally overwhelms the tropical circulation response at the start of CO<sub>2</sub> ramp-down.

After the first few decades of CO<sub>2</sub> ramp-down the equatorial Pacific zonal temperature gradient begins to increase and return to its original level, and this can be attributed to a slowing of the ocean vertical stratification change in this period, combined with a continued increase in the mean tropical circulation. The strength of the Walker circulation also begins to recover during this period, indicating that the influence of the mean tropical circulation has once again become dominant over local ocean stratification changes in the region.

Although spatially non-uniform changes in evaporative damping (Knutson and Manabe 1995) or west Pacific cloud changes (DiNezio et al. 2009) could in theory be important in determining equatorial Pacific SST gradients under CO<sub>2</sub> forcing, there appears to be no reason for either of these to be spontaneously asymmetric with respect to  $T$  during ramp-up/ramp-down because of atmospheric processes alone. As the direct CO<sub>2</sub> forcing simulated in the Hansen experiment doesn't produce large atmospheric circulation changes over the oceans, it seems unlikely that the lag between  $T$  and CO<sub>2</sub> is the root cause of the equatorial Pacific zonal SST gradient changes. Therefore any

influence of evaporation or cloud changes on the SST asymmetries between ramp-up and ramp-down is likely to be a feedback driven by ocean changes.

### 3.6 Sensitivity of results to maximum CO<sub>2</sub> concentration

In order to investigate the robustness and sensitivity to maximum CO<sub>2</sub> concentration of the equatorial Pacific precipitation and SST responses to CO<sub>2</sub> ramp-up/ramp-down, several other experiments were examined. Three HadGEM2-ES experiments increased and decreased CO<sub>2</sub> at 1% per year, similarly to the 4 × CO<sub>2</sub> ramp-up/ramp-down run, but peaked instead at values of 3 × CO<sub>2</sub>, 2 × CO<sub>2</sub> and 1.5 × CO<sub>2</sub>.

As for the 4 × CO<sub>2</sub> experiment, two 40 year periods were chosen for each run with approximately the same climatological mean 1.5 m temperature. The first period was the last 40 years of CO<sub>2</sub> ramp-up, while the second period was during CO<sub>2</sub> ramp-down. Figure 11 shows the difference in precipitation and surface temperature between the two periods for each experiment.

For the 3 × CO<sub>2</sub> and 1.5 × CO<sub>2</sub> experiments the large-scale patterns of precipitation and surface temperature anomalies are similar to the HadGEM2-ES 4 × CO<sub>2</sub> experiment, though the east and central equatorial Pacific positive temperature anomaly is weaker in the 3 × CO<sub>2</sub> experiment. However the 2 × CO<sub>2</sub> experiment shows a very different surface temperature anomaly, with the pattern being dominated by relative warming in the Arctic and cooling in the Antarctic.

This effect is likely to be due to the relative magnitude and lags of the sea-ice feedbacks in the two hemispheres. Whereas for the other ramp-up/ramp-down experiments the lag in sea-ice recovery after peak CO<sub>2</sub> is equal between north and south or larger in the Southern hemisphere, for the 2 × CO<sub>2</sub> experiment the lag is larger in the northern hemisphere (see Fig. 12). This is related to the arctic being relatively warmer in the second 40 year period and in this case dominates the signal in the surface temperature anomaly. The precipitation anomaly in the 2 × CO<sub>2</sub> experiment is also weaker and of a different shape to the other experiments. This is presumably a consequence of the large differences in surface temperature anomaly between this and the other experiments, and indicates that variability in sea-ice feedbacks can have wide-ranging consequences across the globe. The influence of high latitude ice cover on the position of tropical rainfall bands has previously been noted by Chiang and Bitz (2005) and Chiang et al. (2008) in experiments with the Community Climate Model (CCM) version 3 GCM.

As the equatorial Pacific is an area of high natural variability in SSTs and rainfall (Collins et al. 2010; Wu

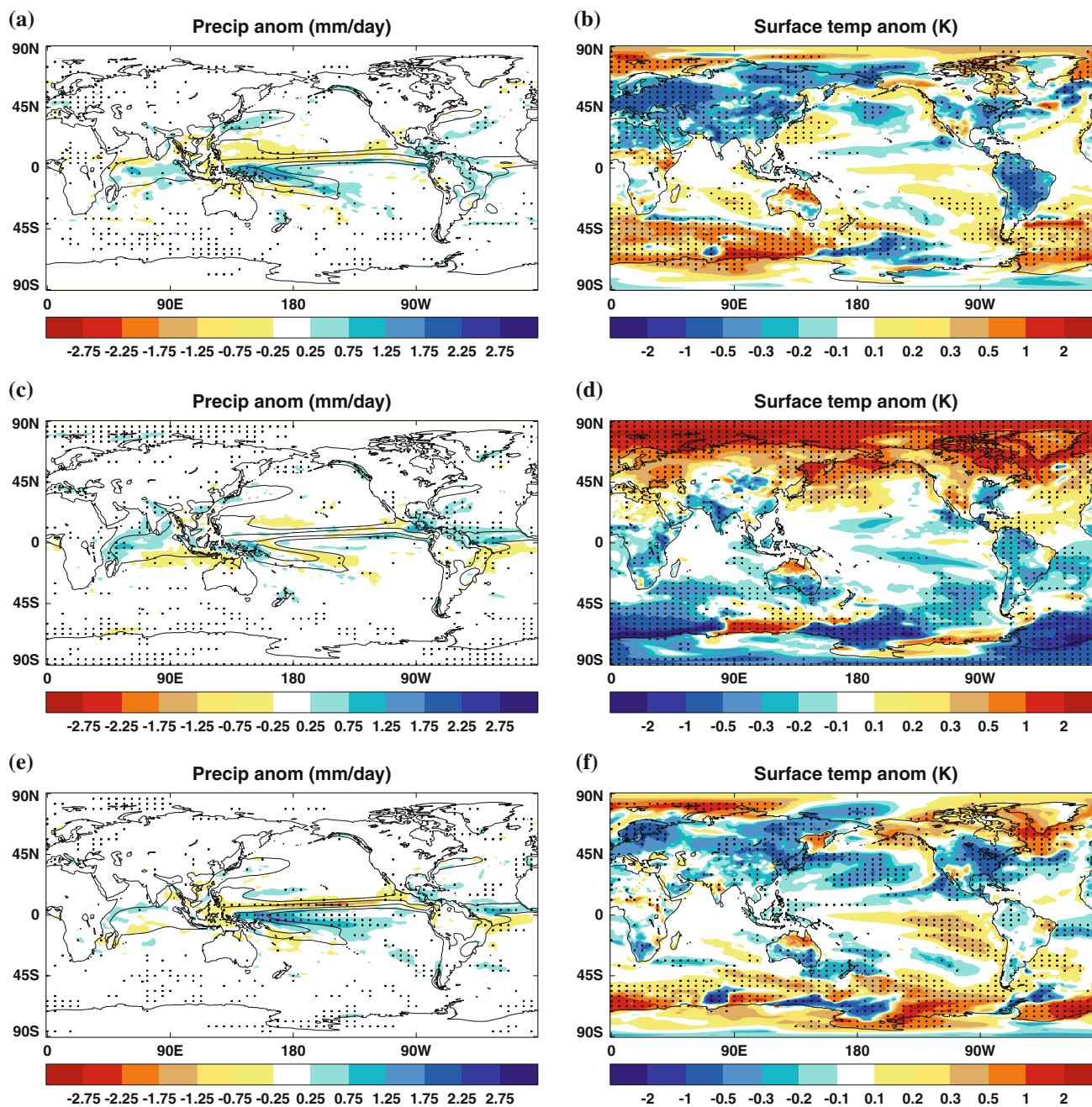
et al. 2003; Matei et al. 2008), much of the differing detail in the responses of the different experiments is likely to be due to this variability. The shape and magnitude of the positive temperature anomaly in the south-east Pacific varies between the different experiments, and is associated with a strong HadGEM2-ES cloud feedback response in this region which will be the focus of a separate study.

Figure 13 shows values of precipitation and temperature averaged between 5°S–5°N for all ramp-up/ramp-down experiments. The mean of the HadGEM2-ES experiments clearly shows an increased equatorial SST gradient across the Pacific and an eastward shift of rainfall from the maritime continent into the Pacific, as does the HadCM3 experiment. Disregarding the HadGEM2-ES 2 × CO<sub>2</sub> experiment, all the other runs show this type of general behaviour with variability in the position of the rainfall anomaly and strength of SST gradient. For HadGEM2-ES the magnitude of the precipitation response does not vary linearly with the magnitude of peak CO<sub>2</sub>, as the 1.5 × CO<sub>2</sub> experiment has a larger Pacific precipitation anomaly than the 3 × CO<sub>2</sub> experiment. Variation in the equatorial Pacific responses of the 4 × CO<sub>2</sub>, 3 × CO<sub>2</sub> and 1.5 × CO<sub>2</sub> experiments is likely to be due to natural variability in what is a highly variable region. The HadCM3 experiment has the largest Pacific SST and precipitation responses, and this may be due to the more abrupt change in forcing between CO<sub>2</sub> ramp-up and ramp-down (2% per year for HadCM3 as opposed to 1% per year for HadGEM2-ES) or simply to inter-model variability.

A decrease in cross-thermocline vertical potential temperature gradient was identified as the likely mechanism for the relative east and central Pacific warming in the 4 × CO<sub>2</sub> ramp-up/ramp-down experiments, and this was also examined for the other ramp-up/ramp-down runs. Figure 14 shows the transient change in thermocline gradient during ramp-up/ramp-down for each of the experiments, and a decrease in gradient during CO<sub>2</sub> ramp-down can be seen in each case. This suggests that the thermocline gradient lag mechanism is not particularly sensitive to the magnitude of maximum CO<sub>2</sub> during CO<sub>2</sub> ramp-up/ramp-down.

### 3.7 Linearity of precipitation and surface temperature responses

As a further test of our understanding, we use the linear simple climate model reconstruction of Good et al. (2011a), applied to HadGEM2-ES (this is not done for HadCM3, due to significant non-linearity in precipitation change identified by Good et al. (2011b)). We do this to test a specific aspect of our proposed mechanism; that the spatial anomaly patterns in Figs. 4 and 11 can be explained solely in terms of different timescales of response in different parts of the



**Fig. 11** Difference (ramp-down minus ramp-up) between two HadGEM2-ES 40 year time periods, one during ramp-down and one during ramp-up, with the same climatological global mean 1.5 m temperature for three different CO<sub>2</sub> ramp-up/ramp-down runs. **a, b** are for 3 × CO<sub>2</sub>, **c, d** for 2 × CO<sub>2</sub> and **e, f** for 1.5 × CO<sub>2</sub>. **a, c,**

**e** Precipitation (mm/day), **b, d, f** surface temperature (K). Grid-points where the anomaly is statistically significant at the 5% level are stippled. *Line contours* indicate mean values during the first 40 year period with contour intervals of 5 mm/day for precipitation and 0.05 Pa/s for convective mass flux

climate system. The linear reconstruction of Good et al. (2011a) aims to predict the spatially-resolved response of a GCM to any given forcing scenario. This method makes a linearity assumption which means that it can reproduce spatial patterns as in Figs. 4 and 11, but only if they arise because of different timescales of response in different parts of the climate system (the hypothesis we wish to test). Any

spatial patterns from non-linear responses will not appear in the linear reconstruction. This reconstruction also has higher signal/noise compared to the equivalent GCM scenario experiment, which allows significant spatial patterns to be identified more clearly.

The reconstruction (described in detail by Good et al. (2011a)) is based on the response of the same GCM to a



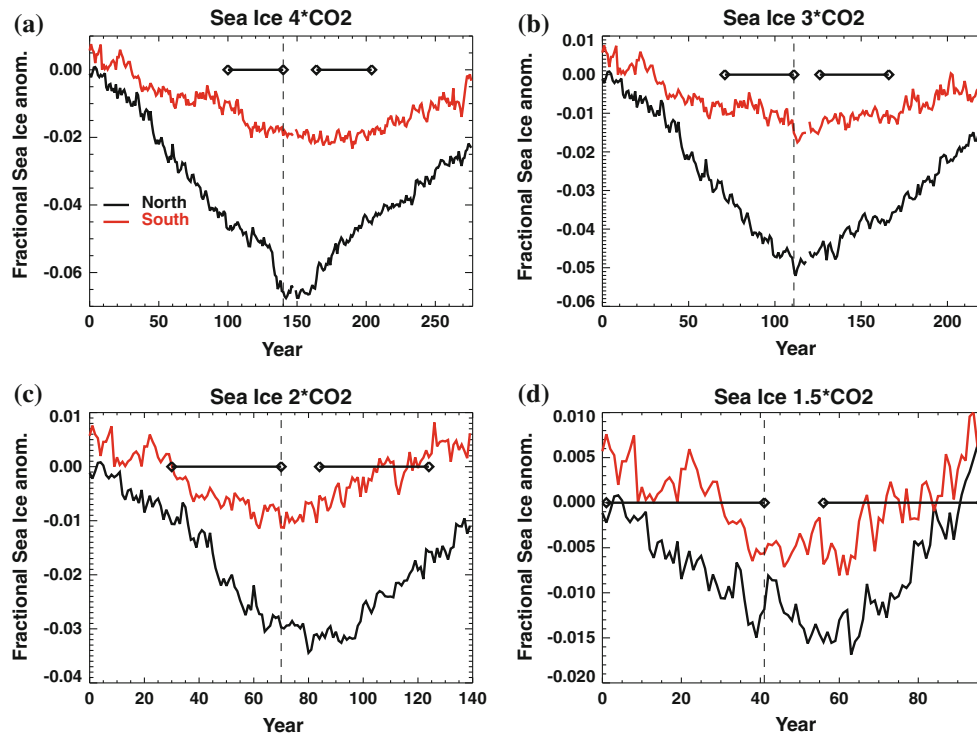


**Fig. 12** Transient changes in anomalous (from control mean) northern (black line) and southern (red line) hemisphere fractional sea-ice coverage for HadGEM2-ES. **a** shows the  $4 \times \text{CO}_2$  experiment, **b**  $3 \times \text{CO}_2$ , **c**  $2 \times \text{CO}_2$  and **d**  $1.5 \times \text{CO}_2$ . Dashed vertical lines show

boundaries of CO<sub>2</sub> ramp-up/ramp-down periods. Horizontal diamond-ended lines signify the position of two time periods with the same climatological global mean  $T$ . Small gaps in the  $4 \times \text{CO}_2$  and  $3 \times \text{CO}_2$  time-series indicate single years of missing data

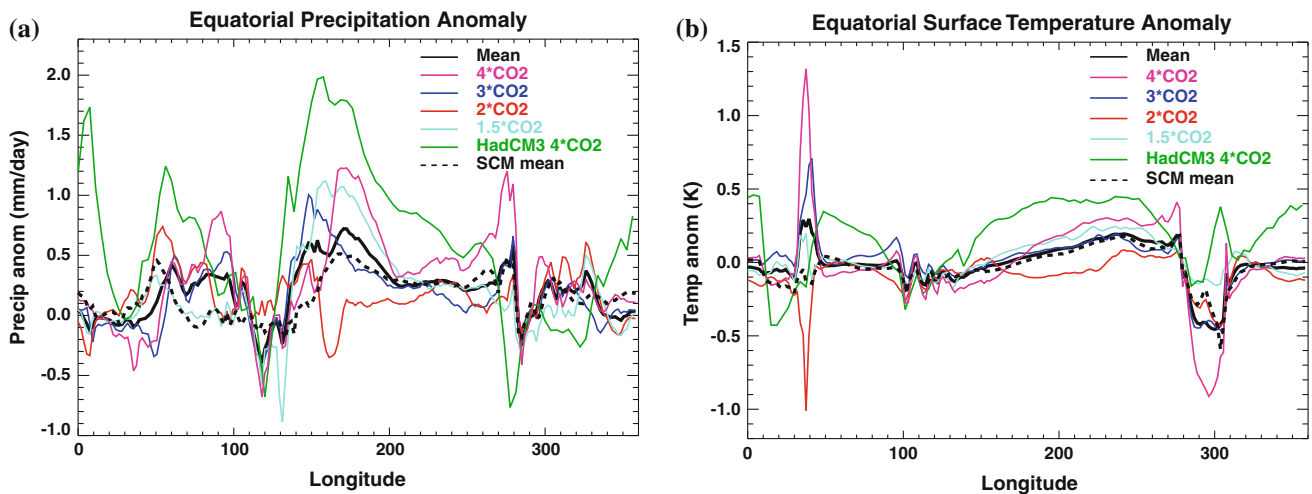


**Fig. 13 a** Precipitation and **b** Surface temperature anomalies (ramp-down minus ramp-up) averaged between 5N and 5S for the difference between two time periods, one during ramp-down and one during ramp-up, with the same climatological global mean 1.5 m temperature. HadGEM2-ES CO<sub>2</sub> ramp-up/ramp-down values are shown for

$4 \times \text{CO}_2$ ,  $3 \times \text{CO}_2$ ,  $2 \times \text{CO}_2$  and  $1.5 \times \text{CO}_2$  experiments, together with the HadCM3  $4 \times \text{CO}_2$  experiment. Thick black solid lines indicate the mean values of all HadGEM2-ES ramp-up/ramp-down experiments. Thick black dashed lines indicate mean value of simple climate model ramp-up/ramp-down simulations

CO<sub>2</sub>-step experiment (where CO<sub>2</sub> is instantaneously increased from pre-industrial concentrations to four times that level and then held constant), combined with a linear assumption. It assumes that the GCM response to any change in forcing is given by a linear scaling of the

response in a CO<sub>2</sub> step experiment, and that the responses to a series of forcing changes are linearly additive.

The results are given in Fig. 15. The reconstruction captures the dominant patterns seen in Figs. 4 and 11. In particular, the reconstruction accurately reproduces the

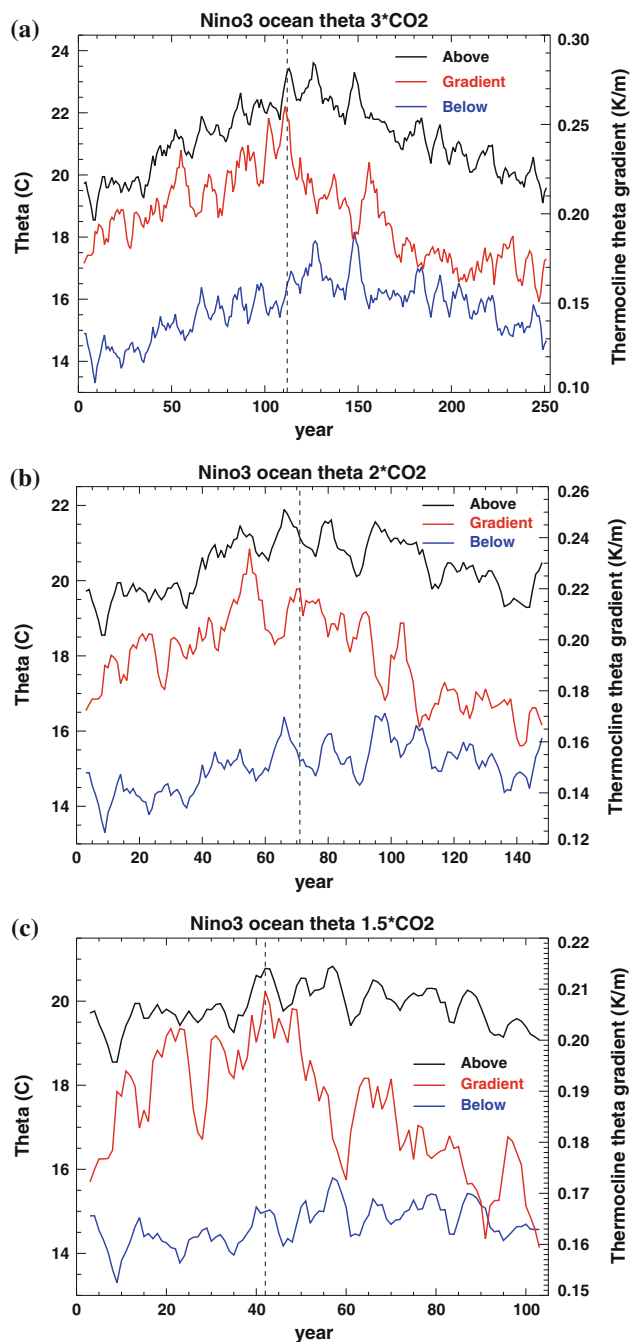


**Fig. 14** Transient changes in mean Niño3 thermocline vertical temperature gradient (K/m) for HadGEM2-ES, as well as the mean temperature of the two model levels above the thermocline and the two model levels below it. **a** shows the  $3 \times \text{CO}_2$  experiment, **b**  $2 \times \text{CO}_2$  and **c**  $1.5 \times \text{CO}_2$ . Dashed vertical lines show boundaries of CO<sub>2</sub> ramp-up/ramp-down periods

HadGEM2-ES ensemble mean near-equatorial signal (compare solid and dashed black lines in Fig. 13). In the case of the simple climate model, unlike HadGEM2-ES, the magnitude of precipitation does increase with the magnitude of peak CO<sub>2</sub> (not shown). This effect may also be present for the GCM, but masked by greater internal

**Fig. 15** Difference (ramp-down minus ramp-up) between two simple climate model simulations of HadGEM2-ES 40 year time periods, one during ramp-down and one during ramp-up, with the same climatological global mean 1.5 m temperature for three different CO<sub>2</sub> ramp-up/ramp-down runs. **a, b** are for  $4 \times \text{CO}_2$ , **c, d** for  $3 \times \text{CO}_2$ , **e, f** for  $2 \times \text{CO}_2$  and **g, h** for  $1.5 \times \text{CO}_2$ . **a, c, e, g** Precipitation (mm/day), **b, d, f, h** surface temperature (K)

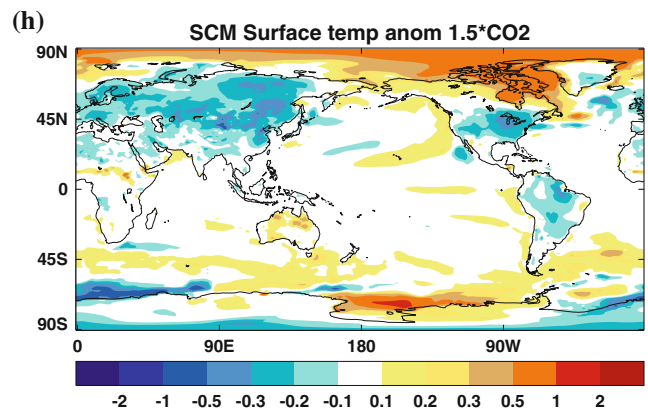
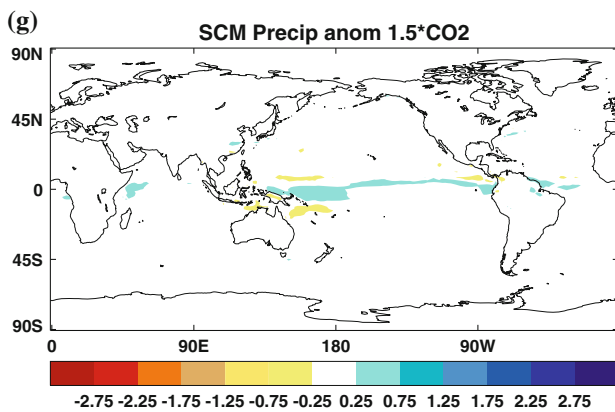
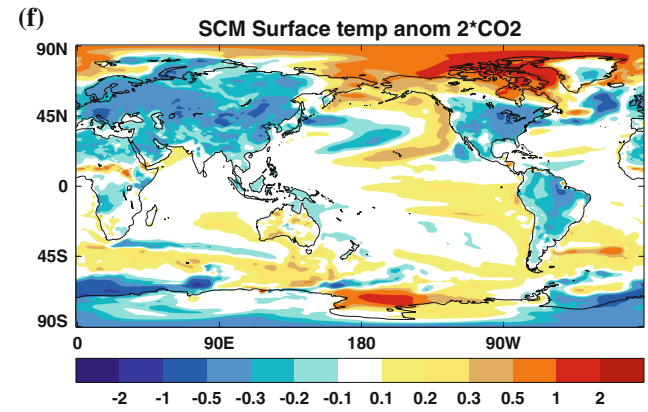
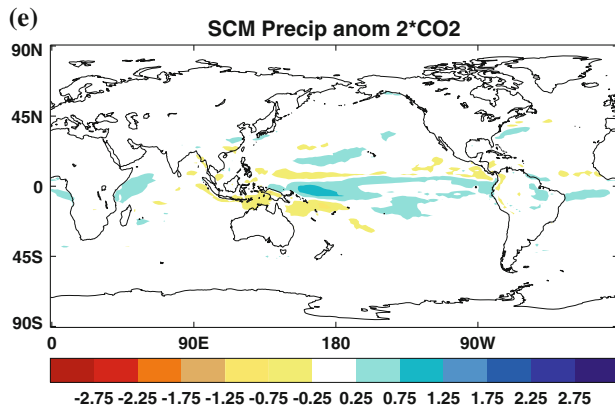
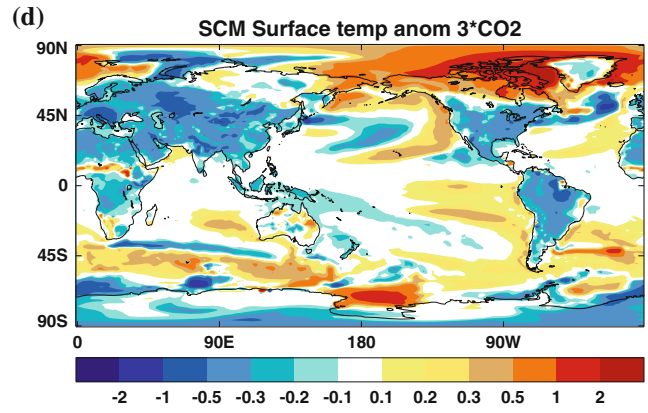
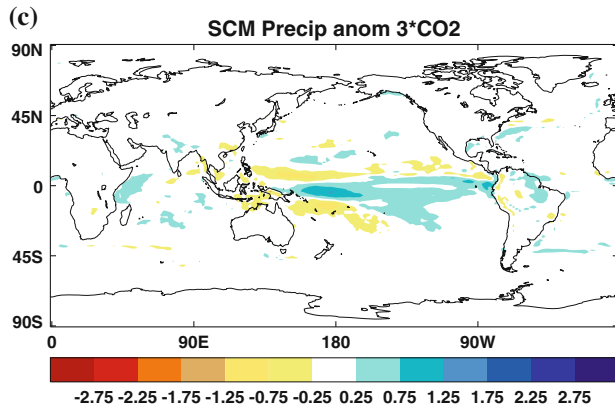
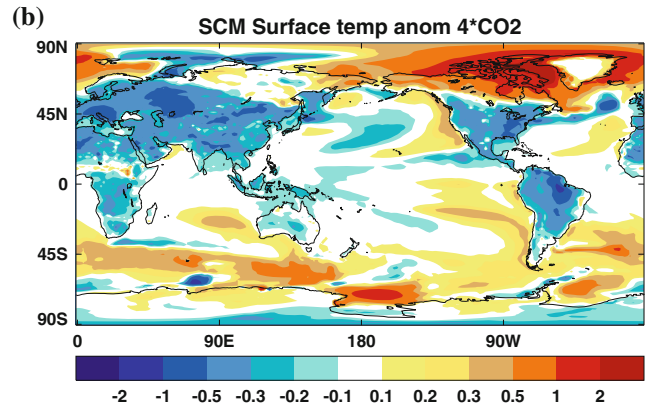
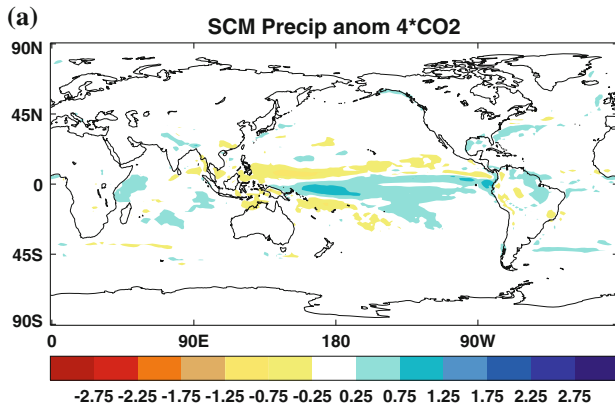
variability. In general the precipitation anomalies are larger in HadGEM2-ES than in the simple climate model, suggesting that non-linear effects (perhaps connected with the coupled Pacific ocean-atmosphere feedbacks) may enhance the linear precipitation signal. Alternatively this could simply be the result of internal variability within the GCM.

The ability of the simple climate model to accurately recreate the GCM response to CO<sub>2</sub> ramp-up/ramp-down suggests that the patterns observed can indeed be explained largely by a linear framework, because of different time-scales of response in different parts of the climate system. In particular, the lagged response between equatorial mixed-layer and sub-thermocline responses to CO<sub>2</sub> forcing that was identified as the mechanism behind the asymmetric equatorial Pacific rainfall and SST patterns is something that the simple model would be expected to capture. The differences between the  $2 \times \text{CO}_2$  ramp-up/ramp-down anomaly patterns and the other experiments seen in HadGEM2-ES is not observed for the simple climate model, adding weight to the argument that non-linear processes such as sea-ice feedbacks are responsible for the behaviour of the  $2 \times \text{CO}_2$  experiment. Again though, the behaviour of the equatorial Pacific in that experiment could also be a consequence of GCM internal variability.

#### 4 Discussion and conclusions

The CO<sub>2</sub> ramp-up/ramp-down experiments described here are highly idealised, and are designed as much to provide insights into the basic mechanisms of the climate system as they are to simulate possible future emissions scenarios. Some relatively simple (and therefore possibly robust across models) rainfall mechanisms associated with a rapid change in the gradient of atmospheric CO<sub>2</sub> emissions are apparent.

A continued increase in global mean rainfall after the start of CO<sub>2</sub> ramp-down can be explained by asymmetry in the speed of reduction of CO<sub>2</sub> and global mean temperature (Wu et al. 2010; Cao et al. 2011). However the asymmetry in rainfall pattern over the tropical Pacific between CO<sub>2</sub> ramp-up and ramp-down is not seen in the Hansen experiment and is therefore unlikely to be due to the direct radiative effect of CO<sub>2</sub>. Instead, slowly evolving heat transfer between the surface and deep ocean appear to be responsible for an east Pacific equatorial SST warming



which continues during CO<sub>2</sub> ramp-down and causes an eastward shift of precipitation.

The magnitude of CO<sub>2</sub>-induced SST warming in the east Pacific is largely determined by the balance between vertical and horizontal heat transport DiNezio et al. (2009). The magnitude of cooling from below is determined by both the strength of upwelling (determined by surface wind stress and associated with the strength of the Pacific Walker cell) and the temperature gradient between the mixed-layer and sub-thermocline waters. Two competing mechanisms are at work here. The first is a reduction in tropical convective mass flux with warming (Held and Soden 2006), which acts to weaken the Walker circulation and reduce upwelling, warming the east Pacific. The second is the ocean thermostat mechanism of Clement et al. (1996), whereby heating of the mixed layer from above increases the cross-thermocline temperature gradient and the efficiency of upwelling-related cooling, thus cooling the East Pacific relative to the rest of the tropics. This thermocline mechanism is controlled by the lag between heating of the surface equatorial waters and the transport of subtropical waters which are heated at the surface, subducted, and upwell in the east Pacific several decades later.

During ramp-up the weakening of the tropical circulation dominates over local stratification changes in the east Pacific in HadGEM2-ES and HadCM3, but the opposite occurs during ramp-down where a local decrease in stratification leads to a continued weakening of the Walker circulation despite both the mean tropical circulation and the Hadley circulation starting to recover. This phenomenon of asymmetric changes in ocean temperature depending on the sign of forcing is also seen in Stouffer (2004) and Yang and Zhu (2011).

Repeating the HadGEM2-ES CO<sub>2</sub> ramp-up/ramp-down experiment with various different maximum levels of CO<sub>2</sub> produced similar results to the 4 × CO<sub>2</sub> experiment for 2 out of 3 runs. However the 2 × CO<sub>2</sub> experiment exhibited a very different relative pattern of surface temperature change between ramp-up and ramp-down, tentatively attributed here to difference in the speed of sea-ice recovery between the two hemispheres. Nevertheless the thermocline lag mechanism appeared to be present in all experiments, and the pattern of tropical precipitation was similar between all but the 2 × CO<sub>2</sub> experiment.

A reconstruction of the HadGEM2-ES ramp-up/ramp-down CO<sub>2</sub> scenarios with a simple linear climate model was able to reproduce the asymmetric patterns of Pacific SST and rainfall with considerable accuracy. This supports the argument that it is different timescales of response in different parts of the climate system (such as between mixed layer and sub-thermocline equatorial waters) that are responsible for the asymmetric pattern responses between CO<sub>2</sub> ramp-up and ramp-down.

Although different GCMs produce a variety of mean equatorial Pacific states under global warming (DiNezio et al. 2009), with some having El-Niño-like SST patterns and others La-Niña-like SST patterns, the mechanism of an ocean-circulation-related lag between heating of the equatorial ocean mixed layer and the sub-thermocline water is a relatively simple one and likely to be present across models. This means that whatever the mean state of the equatorial Pacific in a model during CO<sub>2</sub> ramp-up, the zonal temperature gradient is likely to be weaker at the start of the ramp-down phase of a CO<sub>2</sub> ramp-up/ramp-down experiment than during the ramp-up phase. Held et al. (2010) examined an experiment with the GFDL 2.1 coupled GCM where CO<sub>2</sub> was increased, then instantaneously reduced to pre-industrial levels. They found a residual east Pacific warming after CO<sub>2</sub> reduction, and it seems likely that this is associated with an ocean stratification lag similar to the ones in HadGEM2-ES and HadCM3. In their terminology, this mechanism would be associated with the ‘recalcitrant’ component of warming.

Cao et al. (2011) explain the hysteresis of global mean precipitation during CO<sub>2</sub> ramp-up/ramp-down by the direct dependence of the atmospheric radiation budget on CO<sub>2</sub>. In addition to this another possible mechanism, and one that would merit further investigation, is that the asymmetric patterns of temperature change between ramp-up and ramp-down could alter the atmospheric radiative balance and produce the observed asymmetry in global mean precipitation. For example the land-ocean contrast in heating and cooling could affect the global mean Bowen ratio and distribution of water vapour, and the evolution of SST patterns could produce significant cloud changes. Barsugli et al. (2006) used the NCAR CCM GCM to show that the change in global mean precipitation is sensitive to the pattern of SST warming, not just the tropical mean warming, providing some support for this hypothesis.

The implication of this study is that removing CO<sub>2</sub> from the atmosphere would not return the climate to its pre-industrial state along the same path as during CO<sub>2</sub> increase. Ocean heat content built up during ramp-up would start to be released during ramp-down, and is likely to lead to a warmer mean state in the east Pacific than during ramp-up. This is associated with regional precipitation changes which are likely to have greater human impacts than the lag in global mean *P*. It should therefore not be assumed by policy-makers that a future removal of CO<sub>2</sub> from the atmosphere would stop the climate from changing any further in unexplored ways. As for other forms of geoengineering, global mean temperature alone is a poor metric of the state of the climate system as multiple rainfall climates are possible for the same mean temperature. In particular, pattern-scaling with global mean temperature would be inappropriate for scenarios such as the one here.

There are also implications for a less extreme scenario where CO<sub>2</sub> levels increase and then stabilise. The thermocline lag mechanism would also theoretically occur in this case, though with a smaller magnitude than for CO<sub>2</sub> ramp-down, and this means that observations of transient warming in the equatorial Pacific would show less relative warming in the east Pacific than the final stabilised state.

**Acknowledgments** The authors were supported by the Joint Department of Energy and Climate Change (DECC) and Department for Environment, Food and Rural Affairs (Defra) Met Office Hadley Centre Climate Programme, DECC/Defra (GA01101). We would like to thank Marie Boucher-Boucher for providing the HadGEM2-ES ramp-up/ramp-down data. Thanks also to Mark Ringer, Gill Martin and Graeme Stephens for useful discussions, and to two anonymous reviewers for helpful comments.

## References

- Andrews T, Forster PM, Gregory JM (2009) A surface energy perspective on climate change. *J Climate* 22(10):2557–2570
- Andrews T, Forster PM, Boucher O, Bellouin N, Jones A (2010) Precipitation, radiative forcing and global temperature change. *Geophys Res Lett* 37(L14701)
- Bain CL, De Paz J, Kramer J, Magnusdottir G, Smyth P, Stern H, Wang C-C (2011) Detecting the ITCZ in instantaneous satellite data using spatiotemporal statistical modeling: ITCZ climatology in the East Pacific. *J Climate* 24(1):216–230
- Bala G, Duffy PB, Taylor KE (2008) Impact of geoengineering schemes on the global hydrological cycle. *PNAS* 105(22):7664–7669
- Bala G, Caldeira K, Nemani R (2010) Fast versus slow response in climate change: implications for the global hydrological cycle. *Clim Dyn* 35(2–3):423–434
- Barsugli JJ, Shin SI, Sardeshmukh PD (2006) Sensitivity of global warming to the pattern of tropical ocean warming. *Clim Dyn* 27(5):483–492
- Boucher O, Burke E, Doutriaux-Boucher M, Halloran P, Jones CD, Lowe J, Ringer MA, Wu P (2011) Is the Earth System reversible to climate change? (submitted)
- Cao L, Bala G, Caldeira K (2011) Why is there a short-term increase in global precipitation in response to diminished CO<sub>2</sub> forcing? *Geophys Res Lett* 38(L06703)
- Chiang JC, Bitz CM (2005) Influence of high latitude ice cover on the marine intertropical convergence zone. *Clim Dyn* 25:477–496
- Chiang JC, Fang Y, Chang P (2008) Interhemispheric thermal gradient and tropical Pacific climate. *Geophys Res Lett* 35(L14704)
- Chou C, Neelin J (2004) Mechanisms of global warming impacts on regional tropical precipitation. *J Climate* 17(13):2688–2701
- Chou C, Neelin JD, Chen CA, Tu JY (2009) Evaluating the “Rich-Get-Richer” mechanism in tropical precipitation change under global warming. *J Climate* 22(8):1982–2005
- Clement A, Seager R, Cane M, Zebiak S (1996) An ocean dynamical thermostat. *J Climate* 9(9):2190–2196
- Collins M, An SI, Cai W, Ganachaud A, Guilyardi E, Jin FF, Jochum M, Lengaigne M, Power S, Timmermann A, Vecchi G, Wittenberg A (2010) The impact of global warming on the tropical Pacific ocean and El Niño. *Nat Geosci* 3(6):391–397
- Collins W, Bellouin N, Doutriaux-Boucher M, Gedney N, Halloran P, Hinton T, Hughes J, Jones C, Joshi M, Liddicoat S, Martin G, O’Connor F, Rae J, Senior C, Sitch S, Totterdell I, Wiltshire A, Woodward S (2011) Development and evaluation of an earth-system model—HadGEM2 (submitted to *Geosci Model Dev*)
- DiNezio PN, Clement AC, Vecchi GA, Soden BJ, Kirtman BP (2009) Climate response of the equatorial Pacific to global warming. *J Climate* 22(18):4873–4892
- Gastineau G, Le Treut H, Li L (2008) Hadley circulation changes under global warming conditions indicated by coupled climate models. *Tellus ser A- Dyn Meteorol Oceanogr* 60(5):863–884
- Gastineau G, Li L, Le Treut H (2009) The Hadley and Walker circulation changes in global warming conditions described by idealized atmospheric simulations. *J Climate* 22(14):3993–4013
- Good P, Gregory JM, Lowe JA (2011a) A step-response simple climate model to reconstruct and interpret AOGCM projections. *Geophys Res Lett* 38(L01703)
- Good P, Ingram W, Lambert FH, Lowe JA, Gregory JM, Webb MJ, Ringer MA, Wu P (2011b) A step-response simple climate model for predicting and understanding precipitation from global to regional scales (submitted)
- Gordon C, Cooper C, Senior C, Banks H, Gregory J, Johns T, Mitchell J, Wood R (2000) The simulation of SST, sea ice extents and ocean heat transports in a version of the Hadley Centre coupled model without flux adjustments. *Clim Dyn* 16(2–3):147–168
- Hansen J, Sato M, Ruedy R, Nazarenko L, Lacis A, Schmidt G, Russell G, Aleinov I, Bauer M, Bauer S, Bell N, Cairns B, Canuto V, Chandler M, Cheng Y, Del-Genio A, Faluvegi G, Fleming E, Friend A, Hall T, Jackman C, Kelley M, Kiang N, Koch D, Lean J, Lerner J, Lo K, Menon S, Miller R, Minnis P, Novakov T, Oinas V, Perlwitz J, Perlwitz J, Rind D, Romanou A, Shindell D, Stone P, Sun S, Tausnev N, Thresher D, Wielicki B, Wong T, Yao M, Zhang S (2005) Efficacy of climate forcings. *J Geophys Res Atmos* 110(D18104)
- Held IM, Soden BJ (2006) Robust responses of the hydrological cycle to global warming. *J Climate* 19(21):5686–5699
- Held IM, Winton M, Takahashi K, Delworth T, Zeng F, Vallis GK (2010) Probing the fast and slow components of global warming by returning abruptly to preindustrial forcing. *J Climate* 23(9):2418–2427
- Jones A, Haywood J, Boucher O, Kravitz B, Robock A (2010) Geoengineering by stratospheric SO<sub>2</sub> injection: results from the Met Office HadGEM(2) climate model and comparison with the Goddard Institute for Space Studies ModelE. *Atmos Chem Phys* 10(13):5999–6006
- Karnauskas KB, Seager R, Kaplan A, Kushnir Y, Cane MA (2009) Observed strengthening of the zonal sea surface temperature gradient across the Equatorial Pacific Ocean. *J Climate* 22(16):4316–4321
- Knutson T, Manabe S (1995) Time-mean response over the tropical Pacific to increased CO<sub>2</sub> in a coupled ocean-atmosphere model. *J Climate* 8(9):2181–2199
- Liu Z, Vavrus S, He F, Wen N, Zhong Y (2005) Rethinking tropical ocean response to global warming: the enhanced equatorial warming. *J Climate* 18(22):4684–4700
- Lloyd J, Guilyardi E, Weller H, Slingo J (2009) The role of atmosphere feedbacks during ENSO in the CMIP3 models. *Atmos Sci Lett* 10(3, SI):170–176
- Martin GM, Bellouin N, Collins WJ, Culverwell ID, Halloran PR, Hardiman SC, Hinton TJ, Jones CD, McDonald RE, McLaren AJ, O’Connor FM, Roberts MJ, Rodriguez JM, Woodward S, Best MJ, Brooks ME, Brown AR, Butchart N, Dearden C, Derbyshire SH, Dharssi I, Doutriaux-Boucher M, Edwards JM, Falloon PD, Gedney N, Gray LJ, Hewitt HT, Hobson M, Huddleston MR, Hughes J, Ineson S, Ingram WJ, James PM, Johns TC, Johnson CE, Jones A, Jones CP, Joshi MM, Keen AB, Liddicoat S, Lock AP, Maidens AV, Mannes JC, Milton SF, Rae JGL, Ridley JK, Sellar A, Senior CA, Totterdell IJ, Verhoef

- A, Vidale PL, Wiltshire A (2011) The HadGEM2 family of Met Office unified model climate configurations (to Geosci Model Dev)
- Matei D, Keenlyside N, Latif M, Jungclaus J (2008) Subtropical forcing of tropical Pacific climate and decadal ENSO modulation. *J Climate* 21(18):4691–4709
- McCreary J, Lu P (1994) Interaction between the subtropical and equatorial ocean circulations—the subtropical cell. *J Phys Oceanogr* 24(2):466–497
- McPhaden M, Zhang D (2002) Slowdown of the meridional overturning circulation in the upper Pacific Ocean. *Nat* 415(6872):603–608
- Mitchell J, Wilson C, Cunningham W (1987) On CO<sub>2</sub> climate sensitivity and model dependence of results. *QJRMS* 113(475):293–322
- Pennell C, Reichler T (2011) On the effective number of climate models. *J Climate* 24(9):2358–2367
- Ricke KL, Morgan G, Allen MR (2010) Regional climate response to solar-radiation management. *Nat Geosci* 3(8):537–541
- Robock A, Oman L, Stenchikov GL (2008) Regional climate responses to geoengineering with tropical and Arctic SO<sub>2</sub> injections. *J Geophys Res-Atmospheres* 113(D16101)
- Schubert S, Suarez M, Pegen P, Koster R, Bacmeister J (2004) On the cause of the 1930s Dust Bowl. *Sci* 303(5665):1855–1859
- Seager R, Murtugudde R (1997) Ocean dynamics, thermocline adjustment, and regulation of tropical SST. *J Climate* 10(3):521–534
- Seager R, Naik N, Vecchi GA (2010) Thermodynamic and dynamic mechanisms for large-scale changes in the hydrological cycle in response to global warming. *J Climate* 23(17):4651–4668
- Stouffer R (2004) Time scales of climate response. *J Climate* 17(1):209–217
- Sugi M, Yoshimura J (2004) A mechanism of tropical precipitation change due to CO<sub>2</sub> increase. *J Climate* 17(1):238–243
- Trenberth K, Stepaniak D, Caron J (2000) The global monsoon as seen through the divergent atmospheric circulation. *J Climate* 13(22):3969–3993
- Vecchi G, Soden B, Wittenberg A, Held I, Leetmaa A, Harrison M (2006) Weakening of tropical Pacific atmospheric circulation due to anthropogenic forcing. *Nat* 441(7089):73–76
- Vecchi GA, Soden BJ (2007) Global warming and the weakening of the tropical circulation. *J Climate* 20(17):4316–4340
- Wu L, Liu Z, Gallimore R, Jacob R, Lee D, Zhong Y (2003) Pacific decadal variability: The tropical Pacific mode and the North Pacific mode. *J Climate* 16(8):1101–1120
- Wu P, Wood R, Ridley J, Lowe J (2010) Temporary acceleration of the hydrological cycle in response to a CO<sub>2</sub> rampdown. *Geophys Res Lett* 37(L12705)
- Xie SP, Deser C, Vecchi GA, Ma J, Teng H, Wittenberg AT (2010) Global warming pattern formation: sea surface temperature and rainfall. *J Climate* 23(4):966–986
- Yang H, Zhu J (2011) Equilibrium thermal response timescale of global oceans. *Geophys Res Lett* 38(L14711)
- Zhang M, Song H (2006) Evidence of deceleration of atmospheric vertical overturning circulation over the tropical Pacific. *Geophys Res Lett* 33(12)